JOINT EUROPEAN TORUS

JET–P(92)03

S. Poedts, W. Kerner, J.P. Goedbloed, B. Keegan, G.T.A Huysmans,
E Schwarz and JET Team

Damping of Global Alfven Waves in Tokamaks due to Resonant Absorption

Damping of Global Alfven Waves in Tokamaks due to Resonant Absorption

S. Poedts[1], W. Kerner[2], J.P. Goedbloed[3], B. Keegan[2], G.T.A Huysmans[3], E Schwarz[1] and JET Team*

JET-Joint Undertaking, Culham Science Centre, OX14 3DB, Abingdon, UK

[1]Max-Planck-Institut fiir Plasmaphysik, Garching bei Miinchen, Germany
[2]JET-Joint Undertaking, Culham Science Centre, OX14 3DB, Abingdon, UK
[3]FOM-Instituut voor Plasmafysica "Rijnhuizen", Nieuwegein, Postbus 1207, 3420 BE Nieuwegein, The Netherlands
** See Annex*

Preprint of Paper to be submitted for publication in
Plasma Physics and Controlled Fusion

ABSTRACT.

The MHD spectrum of circular cross-section tokamak plasmas with small aspect ratio is studied for low mode numbers. Particular attention is given to the continuous part of the ideal MHD spectrum of such plasmas. Poloidal mode coupling in finite aspect ratio tokamaks yields gaps in the Alfven continuum. Global Alfven modes are found with a frequency inside these gaps. By interaction with the continuum branches the global Alfven modes experience clamping via phase-mixing. This clamping is computed in resistive MHD. asymptotically small resistivity the clamping is finite and independent of η.

1. Introduction

The gross macroscopic properties of a plasma concerning equilibrium and stability are well described by the theory of magnetohydrodynamics (MHD). In tokamak discharges the plasma evolves through a sequence of MHD equilibria, where the maximum pressure is limited by the stability-, or beta-, limit given by ideal MHD. Non-ideal effects, such as resistivity or viscosity, allow development of slower and weaker instabilities and introduce finite damping in the system.

Additional plasma heating in the form of neutral beam injection or ion cyclotron resonance heating can introduce a strong anisotropy in the plasma pressure. A major effect of energetic ions generated by this heating is the destabilisation of marginally stable ideal MHD modes leading to a burst-like loss of these energetic particles. A prominent example of such an event is the fishbone instability. On the other hand, the interaction of energetic ions and a global MHD mode can lead to enhanced stability. The $m = 1$ mode has been studied extensively. For more details we refer to a recent review by Porcelli (1991).

Additional heating is not the only mechanism to generate energetic particles. The fusion of tritium and deuterium ions produces high-energy α- particles. The confinement of these fusion born α-particles is essential for ignition and hence for the efficiency of generating energy by controlled fusion. It should be added that, strictly speaking, ignition is not required to generate energy. A driven system with high Q is viable. It has been argued by Fu and van Dam (1989a ; 1989b) and Cheng (1990 ; 1991) that these α-particles can destabilise global Alfvén modes and, hence, are lost by the particle-wave resonance. On the other hand, global Alfvén modes experience finite damping in such tokamak plasmas. Since the energetic particles are expected to excite global Alfvén waves, the corresponding energy can also get absorbed through the same physical mechanism which accounts for Alfvén wave heating. In order to find out whether the destabilisation of the global Alfvén waves by the α-particles dominates the damping of these modes by phase-mixing, or vice versa, it is essential to obtain a deeper insight in the Alfvén spectrum of toroidal systems. Therefore, the ideal MHD continuous spectrum needs to be determined for such plasmas and the global Alfvén modes need to be studied in detail. In the present paper, we discuss the results of our investigations of the poloidal mode coupling in the ideal

MHD continuous spectrum, the interaction of the global Alfvén modes with the continuum modes, and the resulting damping of these modes by phase-mixing. The interaction of the energetic particles with the MHD modes is left for a subsequent paper, where the energetic contribution to the change in the potential energy, δW_{hot}, is evaluated in a perturbative way.

It is recalled that the MHD instabilities emerge from the Alfvén branch of the MHD spectrum. The branch of fast magneto-acoustic waves has a strongly stabilizing influence and does, therefore, not couple to unstable MHD modes. The pressure effects which determine the slow magneto-acoustic modes, also do not contribute to the phenomena considered here. We begin the discussion of the Alfvén subspectrum with analytical arguments. Quantitative solutions in toroidal axisymmetric systems are obtained with the normal mode code CASTOR, which solves for the entire spectrum of dissipative MHD (Kerner et al. 1991).

In inhomogeneous systems with cylindrical symmetry, where all equilibrium quantities depend only on the radial coordinate r, singularities occur in the ideal MHD equations if the frequency ω matches the local Alfvén frequency, i.e.

$$\omega = \omega_A(r) = \frac{\vec{k} \cdot \vec{B}_0}{\sqrt{\rho_0}} = \frac{B_\theta}{r\sqrt{\rho_0}} \, (nq(r) + m), \tag{1}$$

where the perturbed quantities have the form

$$f_1(r,t) = f_1(\vec{r}) \; e^{\lambda t} \; e^{im\theta + ink z}, \tag{2}$$

with $\lambda \equiv i\omega$, $\vec{k}$ is the wave vector of the perturbation, $\vec{k} = (0, \frac{m}{r}, nk)$, with poloidal and toroidal wave numbers m and n, $k = 2\pi/L$ defines a periodicity length for modelling a tokamak of aspect ratio $\epsilon^{-1} = \frac{R}{a} = \frac{L}{2\pi a}$, with a the minor radius of the plasma. These singular solutions define the Alfvén continuum. The corresponding eigenfunctions have a logarithmic singularity with a jump contribution at the singular surface in the radial component of the velocity field $v_1 \equiv r v_r$ which results from the analytic continuation of the logarithmic term through the singular point. The poloidal component is basically the radial derivative of v_1, i.e. $v_2 \equiv i v_\theta = -v_1'/m$ for $m \neq 0$, and thus has a $1/(r - r_s)$-singularity and a δ-function contribution. By applying a superposition of these continuum solutions, the mechanism of Alfvén wave heating can be explained in the ideal MHD picture. Here a 'collective' mode is excited by an external antenna which couples to the

shear Alfvén continuum modes. As a result, the energy supplied to the plasma by the external source accumulates in an ever diminishing layer around the singular position $r = r_s$, where the driving frequency matches the local Alfvén frequency $\omega_d = \omega_A(r_s)$. This accumulated energy is thought to be converted into heat by dissipative effects, but this conversion is, of course, beyond the scope of the ideal MHD model. The concept of plasma heating by the resonant absorption of Alfvén waves has been confirmed by calculations in a dissipative system with finite electric conductivity, where the power emitted by the antenna and absorbed by the plasma is actually converted into heat by Ohmic dissipation (Poedts, Kerner & Goossens 1989). The Ohmic dissipation rate ($\sim \int_V \eta j^2 \mathrm{d}V$), however, is not the only important quantity to look at when investigating Alfvén wave heating. The efficiency (or inefficiency) of plasma heating by resonant absorption can be expressed in several complementary ways. A typical figure of merit is the *coupling factor* which is defined as the ratio of the imaginary and the real part of the antenna impedance. Hence, the coupling factor measures the energy that is circulating in the system relative to the absorbed power. An infinite coupling factor means no coupling at all and, hence, no absorption. For efficient plasma heating, a small coupling factor is desirable. However, in engineering terms, the *quality factor* of the resonance, which measures the total energy contained in the plasma relative to the power that is dissipated or absorbed per cycle, is more important. For heating, a low quality resonance, with a lot of dissipation, is prefered. Clearly, a good coupling of the external driver to the plasma does not guarantee a low quality resonance and vice versa. Another important parameter is the *time* the externally excited dissipative system needs *to reach a stationary state* in which the power supplied by the external source is exactly balanced by the Ohmic dissipation rate in the resonant plasma layer(s). This time is directly related to the quality factor. So a large time scale for achieving phase-mixing corresponds to a high quality factor and is not suitable for plasma heating, especially not when the coupling factor is high and, hence, the plasma-driver coupling is bad too.

It was shown (Poedts, Kerner & Goossens 1989) that driving a dissipative system periodically at an arbitrary frequency inside the continuous spectrum often yields only a modest Ohmic dissipation rate (compared to the power emitted by the external source). This is a consequence of the bad coupling of the external driver to the plasma that is obtained with a badly tuned antenna. A better plasma-driver coupling is achieved when a global mode of the system is excited. Such global modes occur in the form of the

stable external kink modes and/or the cylindrical discrete Alfvén waves, which exist only when certain criteria are satisfied (Goedbloed 1984). One of these criteria is that $\omega_A(r)$ has to have an extremum in an internal point, i.e. $\omega'_A(r_{ext}) = 0$. The frequencies ω_i of these discrete modes are located underneath or above the continuous spectrum. Thus, a Sturmian (or anti-Sturmian) sequence of global modes can exist with $\omega_i < min\{\omega_A(r)\}$ (or $\omega_i > max\{\omega_A(r)\}$) and an accumulation point at the end of the continuum. Driving at the frequency of such a discrete Alfvén wave yields extremely good plasma- driver coupling (with a coupling factor of 0, hence 100% coupling) but the time-scale needed to reach the stationary state is also extremely long and, consequently, the quality factor of the resonance is very high, which is bad for heating. Through numerical simulations it was shown that the power emitted by the external source and coupled into the plasma causes a substantial increase of the plasma kinetic and potential energy for a long period of time, while the Ohmic dissipation needs much longer to become important. As a result, the power that is dissipated per cycle in the steady state is relatively small as compared to the total energy contained in the system.

A better candidate for heating and absorption is, therefore, given by the stable external kink with an oscillatory frequency in the range of the ideal Alfvén continuum. For fixed plasma parameters the frequency of the external kink can be adjusted upon varying the distance of the perfectly conducting wall to the plasma. The closer the wall is placed to the plasma, the higher the oscillatory frequency of this mode is. For a certain range of wall positions, the external kink frequency is located in the range of the ideal continuous spectrum. In that case, the frequency is not purely oscillatory any more but, instead, it also has a non-vanishing damping part, i.e. $Re(\lambda) \neq 0$. Therefore, this mode is also called a "quasi-mode" in the literature. The fact that the oscillatory part of the frequency of a quasi-mode is located in the range of the continuum is the essential difference between these discrete modes and the discrete Alfvén waves underneath the continuum mentioned above. Indeed, "quasi-modes" yield good coupling due to their global nature — just as the discrete Alfvén waves — but also efficient heating (with a low quality factor) due to resonant absorption. The relative damping factor δ, defined as $\delta = |\frac{Re(\lambda)}{Im(\lambda)}|$, is affected by the gradient of the local Alfvén frequency and, hence, by the equilibrium profiles. The density profile, in particular, was found to have a substantial influence on this parameter. Clearly, the relative damping factor is inversely proportional to the damping time τ, i.e. the larger δ is, the faster the corresponding mode damps out. It was found that the relative damping

factor can be very large and that the absorption can be very efficient for density profiles with large gradients. We have found cases with δ in excess of 5%. In these calculations the absorption was evaluated within resistive MHD in the limit of asymptotically small η. It was established that the damping and the absorption efficiency, become both independent of η in the limit of small η. This result confirmed that the damping is well defined. Furthermore, the damping is independent of the specific dissipation mechanism.

In tokamak systems the poloidal wave number m is no longer a good quantum number as the finite aspect ratio causes coupling of the different poloidal Fourier harmonics. When continuum branches with the same toroidal wave number but with different poloidal wave numbers (e.g. m and $m+1$) intersect in the cylindrical limit ($\epsilon = 0$), the coupling due to the finite aspect ratio causes an 'avoided crossing' of the two continuum branches considered. Not all frequencies are any longer accessible for the continuum normal modes and, therefore, gaps in the toroidal continua occur. Since the toroidal Alfvén continuum is essential for the further discussion, a new method (Poedts & Schwarz 1991) is applied to determine the toroidal continua accurately and efficiently. Inside the gaps in the toroidal continua discrete frequencies are found which correspond to global Alfvén waves. The coupling of at least two different poloidal Fourier components allows the construction of eigenfunctions where the singularity and the jump are avoided, while satisfying the boundary conditions at the magnetic axis and at the plasma boundary. The oscillatory frequency of these global, toroidicity-induced, Alfvén eigenmodes (so-called TAE modes) is found to be of the order of the typical Alfvén frequency. In the simplest case, these normal modes are truly global, thus the damping in a dissipative system is directly proportional to the dissipation, i.e. for asymptotically small resistivity $\lim_{\eta \longrightarrow 0} \delta = 0$. If, however, the configuration is chosen such that the frequency ω falls into the range of the continuum of a sideband, for example $m+2$, then a finite damping occurs in the limit of asymptotically small resistivity $\lim_{\eta \longrightarrow 0} \delta = \delta_0 \neq 0$, as will be shown in the paper. In other words, the modes have become quasi-modes, similar to the external kink quasi-modes discussed above, but different in nature.

We will concentrate on truly toroidal global Alfvén waves for small aspect ratio, and small toroidal wave number ($|n| \leq 5$), where the leading poloidal harmonic varies from zero to ten. Thereby, our analysis complements recent analytic results based on specific scaling assumptions (Berk et al. 1991 ; Rosenbluth et al. 1991 ; Zorca and Chen 1990).

The physical model considered is presented and discussed in the next Section. In

Section 3 the toroidal Alfvén spectrum is derived with continuum modes and regular, global normal modes. The finite damping which occurs for global Alfvén modes coupling to the continua are discussed in detail in Section 4. Finally, Section 5 presents a discussion of the implication of these results for confinement of fusion born α-particles and recent experiments with anisotropic pressure.

2. Physical model

The dissipation is assumed to be small and, consequently, can be treated in a perturbative manner. This allows application of the usual procedure where the equilibrium is determined by force balance in ideal MHD. The dissipation is then introduced in the motion of small perturbations around the equilibrium state. Here, the dissipation considered is finite electric conductivity. In our previous studies in cylindrical symmetry it has been demonstrated that the dissipative Alfvén spectrum is essentially the same for either viscosity and resistivity as the damping mechanism. Therefore, we are sure that our results, obtained in the limit of asymptotically small resistivity, are indeed independent of the specific dissipation mechanism.

2.1 Equilibrium

Tokamak equilibria obey force balance in ideal MHD

$$\vec{J}_0 \times \vec{B}_0 = \nabla p_0, \tag{3}$$

where $\vec{B}_0$ denotes the equilibrium magnetic field, $\vec{J}_0$ the current density and p_0 the pressure. The magnetic field is represented by the poloidal flux function ψ and the poloidal current profile F

$$\vec{B}_0 = \nabla\phi \times \nabla\psi + F\nabla\phi. \tag{4}$$

Here, the usual flux coordinates (ψ, θ, ϕ) are adopted, with $\psi = \psi(R, Z)$ where (R, Z, ϕ) are cylindrical coordinates. The current density is obtained from the magnetic field

$$\vec{J}_0 = \nabla \times \vec{B}_0. \tag{5}$$

Two profiles, i.e. $p_0(\psi)$ and $F(\psi)$ or $p_0(\psi)$ and $q(\psi)$, together with the shape of the plasma boundary define an equilibrium. The quantity q denotes the safety factor.

A specific equilibrium configuration defines a flux coordinate system (s, ϑ, ϕ) with straight field lines $B_0^\phi / B_0^\vartheta = q(\psi)$. The radial coordinate $s = \sqrt{\psi/\psi_s}$ corresponds to the normalised radius r/a in the cylindrical limit. A suitable choice for the Jacobian is

$$J = \frac{R^2 q}{F}. \tag{6}$$

In addition, the density ρ_0 can be chosen arbitrarily. We make the choice of

$$\rho_0 = \rho_0(s) = \left[1 - (1 - Ds^2)\right]^\nu, \tag{7}$$

with $\nu = 1$ or 2 and the constant D determines the value of the plasma density at the plasma surface, $\rho_0(1) = D^\nu$.

The ideal gas law relates the pressure to the temperature and density

$$p_0 = \frac{\tilde{R}}{\tilde{\mu}} \rho_0 T_0, \tag{8}$$

with $\tilde{R}$ and $\tilde{\mu}$ the Boltzmann constant and the mean molecular weight, respectively. T_0 denotes the equilibrium temperature. The ratio of the averaged plasma pressure and the magnetic pressure defines the plasma beta :

$$\beta = \frac{2\mu \int p_0 \, \mathrm{d}\tau}{\int \vec{B}_0^2 \mathrm{d}\tau}. \tag{9}$$

Another useful expression is the poloidal beta :

$$\beta_p = \frac{2\mu \int p_0 \, \mathrm{d}s}{\left[\int J_{0\phi} \mathrm{d}s\right]^2}. \tag{10}$$

Normalized quantities are introduced, where the distance is normalised to the radius of the magnetic axis R and where the toroidal magnetic field and the plasma density are normalised to their respective values at the axis, viz. $B_{0\phi}(0)$ and $\rho_0(0)$.The electric current density is normalised to $B_{0\phi}/\mu R$ with μ the magnetic permeability.

2.2 Resistive MHD equations

The resistive MHD equations that govern the linear perturbations around the ideal static equilibrium presented above can be written in the (dimensionless) form

$$\frac{\partial \rho_1}{\partial t} = -\nabla \cdot (\rho_0 \vec{v}_1), \tag{11a}$$

$$\rho_0 \frac{\partial \vec{v}_1}{\partial t} = -\nabla p_1 + (\nabla \times \vec{B}_0) \times \vec{B}_1 + (\nabla \times \vec{B}_1) \times \vec{B}_0, \tag{11b}$$

$$\rho_0 \frac{\partial T_1}{\partial t} = -\rho_0 \vec{v}_1 \cdot \nabla T_0 - (\gamma - 1)\rho_0 T_0 \nabla \cdot \vec{v}_1, \tag{11c}$$

$$\frac{\partial \vec{B}_1}{\partial t} = \nabla \times (\vec{v}_1 \times \vec{B}_0) - \nabla \times (\eta \nabla \times \vec{B}_1). \tag{11d}$$

The subscript 1 denotes an Eulerian perturbation. The resistivity, η, is assumed to be constant in the present paper and the ratio of the specific heats, γ, is taken to be 5/3. Equations (11a)-(11d) are, respectively, the continuity equation, the momentum equation for a non-viscous plasma, the equation for the variation of the internal energy, and the induction equation which includes the ohmic term due to the finite electric conductivity of the plasma. An initially divergence-free magnetic field remains divergence-free owing to equation (11d). Notice that there is no restriction to incompressible plasmas. Equations (11a)-(11d) form a system of 8 partial differential equations for 8 unknowns, viz. $\rho_1, v_{1r}, v_{1\vartheta}, v_{1\phi}, T_1, B_{1r}, B_{1\vartheta}$, and $B_{1\phi}$, which is to be completed with appropriate boundary conditions, namely regularity at the magnetic axis $s = 0$ and vanishing normal magnetic field and velocity at the plasma boundary $s = 1$. The system (11) is written in dimensionless form. The time is expressed in Alfvén-transit-times, $t_A = a/V_A$, with $V_A = B_{0\phi}(0)/\sqrt{\mu \rho_0(0)}$. The plasma pressure and the temperature are normalised to, respectively, $B_{0\phi}(0)/\mu$ and $\tilde{\mu} V_A^2/\tilde{R}$. The velocity, $\vec{v}_1$, is normalised to V_A and the resistivity to $\mu\ a\ V_A$ In the following, we will always use dimensionless quantities.

The linearisation of the resistive MHD equations around a static equilibrium is, strictly speaking, an inconsistency in the model since magnetostatic equilibria do not exist in resistive MHD, because the resistive diffusion generates flow. However, linearisation around an ideal magnetostatic equilibrium yields a good approximation for the description of phenomena with a characteristic time scale that is long compared to the dynamic time scale ($\tau_{dyn} = l_0/V_A$, with l_0 a characteristic length) and short compared to the time scale of resistive diffusion ($\tau_{dif} = l_0^2/\eta$). Resonant absorption can be treated within the theory of linear motions around a magnetostatic equilibrium because the characteristic time scale related to this phenomenon is proportional to $\eta^{-1/3}$ and — for the relevant (very small) values of η — much smaller than τ_{dif} ($\sim \eta^{-1}$) but much larger than the dynamic time scale. Put differently, for the very small values of η that are relevant in tokamak plasmas,

τ_{dif} is much longer than the other time scales of interest. Consequently, resistive effects can only be important in localised regions where the current profile has a large gradient, implying a small characteristic length l_0. When the plasma is driven periodically such localised regions form around the ideally singular layers where the local Alfvén frequency matches the frequency of the external source.

Since the equilibrium quantities do not depend on the toroidal angle ϕ the separation ansatz

$$f_1(s,\vartheta,\phi,t) = e^{\lambda\, t} e^{in\phi} f_1(s,\vartheta) = e^{\lambda\, t} e^{in\phi} \sum_{m=-\infty}^{+\infty} f_{1,m}(s) e^{im\vartheta} \tag{12}$$

is suitable for the perturbed quantities. Here, λ is the eigenvalue. The imaginary part of λ corresponds to oscillatory behaviour, while a negative real part indicates damping and a positive real part yields an exponentially growing instability.

MHD spectroscopy (Goedbloed 1991), i.e. the identification of ideal and dissipative MHD modes for the purpose of diagnosing tokamaks and optimising their stability properties, requires a numerical tool which accurately calculates the dissipative MHD spectra for measured equilibria. The new spectral code (Kerner et al. 1991) CASTOR (Complex **A**lfvén **S**pectrum for **TOR**oidal Plasmas), together with the equilibrium solver HELENA (Huysmans, Goedbloed & Kerner 1991), provides such a tool. In CASTOR, the fluid variables $\rho, \vec{v}, T$, and $\vec{B} = \nabla \times \vec{a}$ are discretised by means of a combination of cubic Hermite and quadratic finite elements for the radial direction and Fourier modes for the poloidal coordinate. The equilibrium in non-orthogonal flux coordinates (ψ, ϑ, ϕ) with straight field lines is computed using isoparametric bicubic Hermite elements, resulting in a very accurate representation of the metric elements. Finally, for analysis of JET discharges the equilibrium solver HELENA is interfaced with the equilibrium identification code IDENTC(D).

In the absence of particle effects, the resulting generalised non-symmetric eigenvalue problem $\mathbf{A} \cdot \vec{x} = \lambda\ \mathbf{B} \cdot \vec{x}$ with block tridiagonal matrices $\mathbf{A}$ and $\mathbf{B}$ is solved by means of different algorithms (QR, inverse vector iteration, Lanczos) which produce the complete spectrum, single eigenvalues, or branches of the spectrum in the complex λ-plane, respectively. The structure of the code allows for easy extension with other dissipative terms.

e.g. viscosity and thermal conductivity.

3. Toroidal Alfvén Spectrum

3.1 Continuous spectrum

In ideal MHD the Alfvén spectrum of tokamak plasmas comprises both discrete and continuous spectra. The corresponding continuous "normal" modes are characterised by non-square integrable singularities. When the equilibrium quantities depend only on the radial coordinate, being constant on magnetic surfaces, different poloidal Fourier components of the perturbations, Eq. (12), do not couple and the continuous part of the spectrum is determined easily by the coefficient of the highest radial derivative acting on the normal component of $\vec{v}$. The condition that this coefficient vanishes yields the dispersion relation Eq. (1) in a simple algebraic form. Generally, in toroidal systems the equilibrium quantities exhibit poloidal dependence. This loss of symmetry makes the determination of the continuous spectrum more complicated by introducing derivatives in the poloidal direction. Goedbloed (1975) and Pao (1975) have shown that the continuous spectrum is determined by a reduced eigenvalue problem in the form of a fourth-order system of ordinary differential equations on each flux surface. This analysis utilises an expansion at a particular flux surface $\psi = \psi_S$. This reduced eigenvalue problem yields a discrete set of eigenvalues on each flux surface. When the position of the flux surface is varied each eigenvalue of this discrete set maps out a continuous spectrum. It has been shown, in addition, that the normal components of velocity and magnetic field possess a logarithmic singularity while the perpendicular components diverge as $1/(\psi - \psi_S)$.

We have found an extremely convenient way for computing the continuous sub-spectra (Poedts & Schwarz 1991). It is recalled that the numerical solution of the MHD equations in the form of a normal mode analysis leads to a large-scale eigenvalue problem $\mathbf{A}\cdot\vec{x} = \lambda\,\mathbf{B}\cdot\vec{x}$, where $\vec{x}$ stands for the numerical coefficients of the state vector $\vec{W}^T = (\rho_1, \vec{v}_1, T_1, \vec{a}_1)$, where $\vec{B}_1 = \nabla \times \vec{a}_1$. By supplying sufficiently many poloidal harmonics M and radial points N_ψ the entire spectrum — the continuous part as well as discrete modes — is computed. This, however, requires the solution of large-scale eigenvalue problems with dimension up to 50,000. The amount of computational work necessary to map out the continua can be decreased significantly by solving a reduced eigenvalue problem on each

flux surface separately. Instead of solving for the singular behaviour in the eigenfunction by means of a large number of radial grid points, the known singular nature is prescribed and it is solved for the remaining regular part. This is achieved by utilising the sub-blocks of CASTOR within the matrices **A** and **B** but replacing the finite elements for representing the normal components of $\vec{v}_1$ and $\log(\tilde{\epsilon})$ and the corresponding elements for the remaining components of the state vector by $1/\tilde{\epsilon}$, where the constant $\tilde{\epsilon}$ has a small value, typically $\tilde{\epsilon} = 10^{-8}$. This reduced eigenvalue problem on each flux surface is solved very accurately and efficiently by the QR algorithm.

A circular cross-section equilibrium with aspect ratio $\epsilon^{-1} = 2.5$, a safety factor increasing monotonically from $q_0 = 1.10$ on the magnetic axis to $q_S = 2.66$ at the plasma surface (as indicated in Fig. 1a) and with a small pressure $\beta_p \approx 2\%$ and $\beta \approx 0.06\%$ is analysed. The density is only slightly varying with $D = 0.5$ and $\nu = 2$ in Eq. (8). The toroidal wave number is chosen as $n = -1$ and five poloidal harmonics are included, viz. $m = 0$, 1, 2, 3, and 4. Part of the continuous spectrum is displayed in Fig. 1a. The profiles of the local Alfvén frequencies are shown in dependence of the radial coordinate s. The dominant poloidal Fourier harmonic is indicated on each continuum branch. The slow magnetosonic continua are in this case close to the origin (as a consequence of the considered low plasma pressure), whereas the frequencies of the Alfvén continuum modes readily exceed unity.

The branch of the predominantly $m = 1 (m = 2)$ mode extends with increasing s from $Im(\lambda) = 0.10$ to $Im(\lambda) = 1.64$ (from $Im(\lambda) = 0.82$ to $Im(\lambda) = 0$, respectively). There is a finite gap around $Im(\lambda) \approx 0.5$ induced by poloidal mode coupling. The mode coupling between the $m = 1$ and $m = 2$ components is the strongest at $s = 0.72$, where the safety factor is $q = 1.50$. The resulting gap in the continuous spectrum reaches from $Im(\lambda) = 0.33$ to $Im(\lambda) = 0.65$. In the cylindrical limit ($\epsilon = 0$) this coupling between the $m = 1$ and the $m = 2$ mode vanishes producing two independent continua for $m = 1$ and $m = 2$ with a degenerate continuum frequency at the rational surface where $q = 1.50$. Near the plasma boundary, at the rational surface where $q = 2.5$ ($s = 0.98$), toroidicity- induced poloidal mode coupling between the $m = 2$ and the $m = 3$ modes causes a similar 'avoided crossing' in the continuum branches of the predominantly $m = 2$ and 3 components. The resulting gap in the continuous spectrum overlays the previous one and reaches from $Im(\lambda) = 0.23$ to $Im(\lambda) = 0.73$. Three other gaps are visible in the window shown in Fig. 1a, one around $Im(\lambda) = 1.0$ and two around $Im(\lambda) = 1.5$. These gaps are much smaller than the

previous ones because they result from the coupling of 'non-neighbouring' poloidal modes, i.e. $\mid m - m' \mid \neq 1$. As the mode coupling is gradually weaker with increasing $\mid m - m' \mid$, the corresponding gaps are gradually smaller. The gap at $s = 0.91$, for instance, is due to the coupling of the $m = 1$ and 3 harmonics, which is strongest at $q = 2.0$. This gap is smaller than the previous ones : it reaches from $Im(\lambda) = 0.94$ to $Im(\lambda) = 1.11$. Still smaller are the two gaps around $Im(\lambda) = 1.5$: one at $s = 0.72$ reaching from $Im(\lambda) = 1.48$ to $Im(\lambda) = 1.50$ and one at $s = 0.98$ reaching from $Im(\lambda) = 1.51$ to $Im(\lambda) = 1.60$. These gaps are due to the next higher order in the mode coupling, namely between the $m = 0$ and 3 components at $s = 0.72$ (where $q = 1.5$) and between the $m = 1$ and 4 harmonics at $s = 0.98$ (where $q = 2.5$).

Fig. 1b displays the corresponding part of the full ideal MHD spectrum computed with CASTOR with only 21 radial grid points and for the same poloidal mode numbers. Of course, CASTOR can not determine the internal structure of the continuous spectrum, i.e. the radial profiles of the local Alfvén frequencies. Instead, the projection of these profiles on the imaginary λ-axis is obtained with CASTOR. The continuous part of the spectrum as well as the related gap structure corresponds satisfactorily for the two procedures. For a full agreement, of course, the same number of radial grid points should be provided in both procedures, which would require the inverse iteration technique for one eigenvalue at a time as the QR algorithm, which diagonalises the entire matrix, is then no longer applicable because of its enormous memory requirements. It is, nevertheless, evident from Fig. 1a and b that the two spectra agree well on the continuum branches. The apparent discrepancy near $Im(\lambda) \leq 0.94$ and 2.0 is due to the coarse grid in the complete solver using only $N_\psi = 21$ grid points and thereby resolving only few continuum modes. For Fig. 1a the reduced eigenvalue problem was solved on 400 (equidistant) magnetic flux surfaces.

3.2 Discrete global modes

Inspection of the location of the singular surfaces of the continuum modes reveals indeed full agreement with the sub-spectra in Fig. 1a. This confirms the existence of "forbidden zones" in the eigenvalue plane as can be established easily in the large-aspect ratio limit by keeping at least two Fourier harmonics. Fig. 1b reveals, in addition, the existence of discrete global modes within these forbidden zones (Cheng & Chance 1986), here for $Im(\lambda) = 0.39$ and $Im(\lambda) = 0.95$. The Real part of the rv_r- component of the

eigenfunction of the discrete Alfvén mode in the basic gap is shown in Fig. 2. In addition to the expected $m = 1$ and 2 components the $m = 3$ and 4 components show up too, with a smaller amplitude due to the small aspect ratio ($\epsilon = 0.4$). It is evident that the discrete gap mode extends throughout the plasma. This indicates that the mode coupling allows the construction of discrete normal modes, which avoid the jumps and singularities that are present in the cylindrical limit ($\epsilon^{-1} = \infty$) and which satisfy the boundary conditions. An immediate conclusion is that there should be more than one discrete global mode with this property as many poloidal modes couple. We expect an entire class of global Alfvén modes with increasing number of radial nodes. On the other hand, not in every gap such a global mode occurs. Gap modes only appear when the poloidal mode coupling is strong enough. For instance, in Fig. 1 such a mode is missing in the small gap ('small' because of weak mode coupling) around $Im(\lambda) = 1.5$. But, as we will see, even with strong mode coupling the resulting gaps can be 'empty'.

The frequencies of these discrete gap modes and, hence, the position of these frequencies in the gaps, depend clearly on the specific equilibrium. By changing the equilibrium parameters, for instance by increasing the pressure and/or by decreasing the inverse aspect ratio $\epsilon^{-1} \longrightarrow 1.0$, the eigenvalue corresponding to the gap mode can even be 'pushed' outside the gap. This is demonstrated in Fig. 3 where a set of equilibria is considered with increasing pressure. In Fig. 3 the relative distance of the gap mode frequency to the lower edge of the gap in which it is located, is displayed versus the poloidal plasma beta, β_p (see eq. 10), of the equilibrium. It is seen that the gap mode shifts towards the lower edge of the gap as the plasma pressure is increased. For $\beta_p = 1.27$ the mode sits on the lower edge of the gap and for still higher plasma pressure it seems to disappear out of the gap into the continuous spectrum where it couples to the continuum modes (the mode indicated on the plot is the one the code converged to, but at this moment it is not clear to us whether this is an ordinary continuum mode or whether the gap mode has maintained its discrete character even at this point outside the gap).

In order to demonstrate the other extreme, namely the fact that a single gap can contain more than one global mode at once, we found it more effective to vary the aspect ratio. We enhanced the poloidal mode coupling due to toroidicity by increasing the toroidicity effect, i.e. by increasing the inverse aspect ratio of the equilibrium. As a result of the increasingly stronger mode coupling the gap size gradually increases as illustrated in Fig. 4, where the lower and upper edges of the basic gap are plotted versus the inverse

aspect ratio ϵ. Also indicated here are the corresponding frequencies of the discrete gap modes found in this gap. When the gap is wide enough, i.e. when the poloidal mode coupling is strong enough, a second gap mode appears in the basic gap. For the case shown in Fig. 4 this happens for $\epsilon = 0.6$. We made a convergence study of the frequency of this second gap mode for $\epsilon = 0.8$, both in N_ψ and N_m, in order to check whether this second gap mode is not an artefact caused by a too low resolution or a too small number of Fourier harmonics (for $\epsilon = 0.8$ the poloidal mode coupling is quite strong and 5 modes do not suffice to represent the mode accurately). We went up to 100 radial intervals and 11 Fourier components ($m = -3 \rightarrow 8$) and obtained full convergence with the frequency still in the gap which proves there are indeed two modes in this gap. The second gap mode looks different than the first one which looks very similar to the mode shown in Fig. 2. The real part of the rv_r-component of the eigenfunction of the second gap mode is displayed in Fig. 5. It is seen that the dominant $m = 2$ component of this mode has one radial node in the rv_r-component in contrast to the first gap mode (see Fig. 2). It is also seen that this mode has a different parity in the Fourier harmonics. For the mode shown in Fig. 2, all coefficients of the Fourier harmonics have the same sign whereas for the mode shown in Fig. 5, these signs are not all the same. The same applies to the other components of the eigenfunction. The $m = 2$ contribution is dominant and all coefficients of Fourier modes with $m > 2$ have the same sign as the $m = 2$ component, while those of the harmonics with $m < 2$ all have the opposite sign.

3.3 High-n cases

A gradually more complex gap structure emerges in the continuous spectrum for a stronger magnetic shear, stronger density variation and higher toroidal mode number. Again the circular cross-section tokamak with aspect ratio $\epsilon^{-1} = 2.5$ is analysed having small pressure and a safety factor increasing from $q_0 = 1.05$ on axis to $q_S = 2.54$ on surface. Now, the toroidal wave number is chosen as $n = -3$ and the poloidal wave numbers are $m = 2, 3, 4, 5$, and 6. The density profile considered here is given by equation (8) with $D = 0.05$ and $\nu = 2$. The continuum structure and the corresponding part of the entire ideal-MHD spectrum are shown in Figs. 6a and 6b, respectively. The $q(\psi)$-profile is also indicated on Fig. 6a. Again, the numbers on the contnuum branches indicate the dominate Fourier harmonic for that continuum branch. Three overlaying gaps with $Im(\lambda) \approx 0.5$ occur : near $s = 0.47$ where $q = 7/6$ and $m = 3$ and 4 couple strongly, near $s = 0.78$ where

$q = 1.5$ and $m = 4$ and 5 couple strongly, and near $s = 0.89$ where $q = 11/6$ and $m = 5$ and 6 couple strongly. From Fig. 6b it is clear that two discrete, global Alfvén waves exist in these gaps. The ideal MHD eigenfrequencies of these two modes are indicated in Fig. 6b and the rv_r-components of the corresponding eigenfunctions are displayed in Figs. 7a and 7b. Two other gaps occur around $Im(\lambda) = 1.0$ due to the coupling of the $m = 3$ and 5 modes (at the $q = 4/3$-surface) and the $m = 4$ and 6 modes (at the $q = 5/3$-surface). The calculation of the ideal MHD spectrum by means of the QR algorithm seems to suggest the existence of a global wave inside the $m = 3, m = 5$ gap (see indication on Fig. 6b). This, however, is a consequence of the low spatial resolution imposed by the enormous memory requirements of the QR algorithm. An inverse vector iteration with higher resolution ($N_\psi = 101$) reveals that the indicated frequency corresponds to a continuum mode and not to a global mode. Indeed, the $m = 4$, 5 and 6 continuum branches in the outer part of the plasma cover the $m = 3, m = 5$ gap at the $q = 4/3$-surface (see Fig. 6a). The low spatial resolution used to produce Fig. 6b is responsible for the bad representation of these continuum branches. Hence, only two gap modes are found in this configuration. In contrast to the previously shown gap modes, these global modes interact now with the continua because the gaps in which they are located are now overlayed by one or more continuum branches which is a consequence of the steep density profile near the plasma surface ($D = 0.05$). The two discrete global modes in the lower gaps both exhibit a singular $m = 6$ component due to coupling to the $m = 6$ continuum branch that is overlaying these gaps (see Fig. 6a), whereas the regular gap modes are mainly due to coupling of the $m = 3$ and 4 and $m = 4$ and 5 harmonics, respectively. The consequences of the coupling between the discrete global modes and the (singular) continuum modes yielding singular parts in the eigenfunctions is discussed in the next Section.

An even more pronounced gap structure is obtained for $n = -5$ as shown in Fig. 8. Here the equilibrium parameters are chosen such that the interaction of the gap modes with the continua are not pronounced. In Fig. 8 many more gaps occur as compared to the previously shown continua. This is a consequence of the higher $|n|$-value. Remember that the gaps occur in toroidal plasmas on the rational surfaces where $q = \frac{-(m+m')}{2n}$ as a result of the cancellation of the one-dimensional degeneracies on those surfaces. For higher n-values there are gradually more of such rational surfaces and, hence, there are gradually more gaps in the continuous spectrum. In Fig. 8 not less than 8 overlying gaps occur around $Im(\lambda) = 0.5$ due to coupling of the $m = 5$ and the $m = 6$ branch at $s = 0.32$

(where $q = 11/10$), the $m = 6$ and the $m = 7$ branch at $q = 13/10$, etc. The same scenario is repeated around $Im(\lambda) = 1.0$ due to the (higher order) coupling of dominant modes with a poloidal mode number that differs by 2 ($m = 5$ and 7, 6 and 8, etc.). Notice also in Fig. 8 that the width of the gaps depends clearly on the magnetic shear : the gap size increases with increasing q-values.

The findings of this Section reveal that for tokamak configurations there exist gaps, i.e. forbidden eigenvalues, in the ideal MHD continuous spectrum. These gaps are due to toroidal effects which couple continuum branches with different poloidal wave numbers m and m'. This coupling is the strongest at the rational surfaces where the corresponding one-dimensonal continuum frequencies are degenerate, i.e. where $q = -(m + m')/2n$. The effect of the mode coupling is to cancel these degeneracies which results in 'crossing avoidances' and, hence, gaps. In addition, there exists a class of discrete global Alfvén modes with eigenfrequencies within these gaps due to toroidal coupling.

4. Damping of Global Alfvén Waves

Regular discrete Alfvén modes possess a well defined frequency and in such a mode every part of the plasma oscillates with this particular frequency. For a continuum mode, on the other hand, it holds that the normal component of the velocity is damped like $1/t$

$$v_n \sim \omega_A e^{-\omega_A t}/t, \tag{13}$$

whereas the tangential components execute undamped oscillations

$$v_t \sim -i(\omega_A \omega'_A/k_\perp)e^{-\omega_A t}. \tag{14}$$

These components undergo completely uncoordinated oscillations, where each plasma layer oscillates with its own local Alfvén frequency. If the plasma is continuously excited periodically at such a continuum frequency, phase-mixing takes place until eventually after a time τ_{SS} a steady state is reached and the entire plasma oscillates with the same driving frequency $\omega = \omega_d$. As a consequence of the phase-mixing, the oscillation of neighbouring flux surfaces with different local Alfvén frequencies gets out of phase and large gradients build up around the plasma layer where the local Alfvén frequency matches the frequency of the external driver. In this resonant layer dissipative effects become important. Hence,

the damping of Alfvén waves by phase-mixing is essentially due to the inhomogeneity of the equilibrium in ordinary space and is analogous to Landau damping which results from the inhomogeneity of the equilibrium in velocity space. The efficiency of plasma heating by phase-mixing or resonant absorption is completely determined by the presence of global discrete modes with a frequency in the range of the ideal continuous spectrum. These modes play the role of energy-carrier and transport the energy supplied by the external source from the plasma surface, through the magnetic surfaces, to the resonant layer. As shear Alfvén waves propagate only along magnetic field lines, resonant absorption is highly inefficient without such a damped global mode. Since the ideal MHD differential operator is Hermitian, there exist no eigenfrequencies with both a non- vanishing real and imaginary part. Therefore, this mode of plasma oscillation does not correspond to a normal mode in ideal MHD and is consequently called a "quasi-mode" or "collective mode". In a previous paper (Poedts & Kerner 1991) it has been shown that the ideal quasi-modes correspond to weakly damped eigenmodes of the resistive-MHD differential operator. Moreover, in the limit of vanishing plasma resistivity the damping of these resistive eigenmodes remains finite and becomes independent of the plasma resistivity. Hence, these resistive eigenmodes converge to their ideal-MHD analogues in the limit of vanishing η. It is emphazised that this does not hold for the Alfvén continuum modes. In resistive MHD, the ideal continuum is replaced by a set of discrete resistive eigenvalues which lie on well-defined curves in the complex λ-plane. With a finite number of exceptions these resistive eigenmodes do not converge to the ideal MHD continuum modes in the limit of asymptotically small resistivity.

In the following we will construct global Alfvén modes interacting with continuum modes by choosing the equilibrium parameters such that there is a continuum branch overlaying the gap, so that the gap mode frequency corresponds to the local Alfvén frequency of at least one magnetic surface. In analogy to the calculation in cylindrical geometry the singularity in the equations is removed by including finite resistivity. Again, the resulting damping is determined by computing $Re(\lambda)$ in a resistive plasma and then decreasing the plasma resistivity. Since the damping becomes independent of the actual value of the resistivity in the limit of vanishing eta, we are again dealing with quasi-modes but this time in toroidal systems. It has been shown above how the gap structure is changed by varying the magnetic shear and the density profile. By changing the constant D for the equilibrium studied in Fig. 1 from $D = 0.5$ to $D = 0.01$, the density decreases strongly in the outer

part of the plasma causing a strong increase in the local Alfvén frequency. The resulting gap structure is displayed in Fig. 9. There is only one gap visible in the window shown in Fig. 9. It results from a crossing avoidance of the two continuum branches with, respectively, $m = 1$ and $m = 2$ as dominant Fourier harmonic and extends form $Im(\lambda) = 0.525$ to $Im(\lambda) = 0.819$. A global Alfvén mode is found with $Im(\lambda) = 0.58$ (in the gap). Notice however, that due to the strong density decrease in the outer part of the plasma the $m = 2$ branch increases again in this part of the plasma and overlays the gap. As a result, the gap mode frequency matches now a continuum frequency on the $m = 2$ branch near the boundary. This, of course, affects the eigenfunction corresponding to the gap mode. The eigenfunction for ideal MHD, i.e. $\eta \equiv 0$, (see Fig. 10a) reveals a regular, global plasma mode with a singular behaviour at $s = 0.94$. It is evident that all Fourier components, not only the $m = 2$ component, couple to the singularity. A physical eigenmode without singularity is obtained for finite resistivity, $\eta \equiv 10^{-7}$ (shown in Fig. 10b). Due to the low resistivity the solution is nearly singular. So, the regular part in the eigenfunction is identical as in ideal MHD (see Fig. 10a) and the solution is changed only in a small layer around $s = 0.94$. The singular behaviour of the ideal MHD eigenfunction is clearly recognizable in the resistive solution and the jump contribution even appears more pronounced although their is no real jump any more. It has to be pointed out that for the considered equilibria with up- down symmetry the matrices **A** and **B** in the eigenvalue problem have real elements. Therefore, a complex eigenfunction is required for an imaginary or complex eigenvalue. For these eigenmodes, the jump and the logarithmic singularity in the normal component of the velocity manifest themselves more dominantly in either the real part or in the imaginary part of the complex eigenfunction. This fact explains why in Fig. 10a, the logarithmic singularity is more pronounced and in Fig. 10b, the jump.

Next, it has to be examined how the results and, in particular, the damping that follows from the coupling to the continuum modes, depend on the actual value of eta. In Fig. 11 a convergence study of the damping ($|\ Re(\lambda)|$) of the gap mode shown in Fig. 10 is presented. This figure shows in fact two kinds of convergence at once, viz. convergence of the damping for $\eta \longrightarrow 0$ and, for each value of η convergence with respect to the N_ψ. The plasma resistivity η was varied over four orders of magnitude from 10^{-4} to 10^{-8} and the damping has been computed with 51, 101, 201, 401, 601, and 801 spatial grid points in radial direction for each eta value. It is clear that sufficiently many radial mesh points are required for properly resolving the (nearly-singular) layer around $s = 0.94$. It is also

clear that this resolution has to be higher for lower values of the plasma resistivity since the layer is narrower than. This qualitative picture is indeed confirmed and quantified in Fig. 11. For $\eta = 10^{-4}$ and 10^{-5}, 51 radial grid points are sufficient and increasing the resolution just yields exactly the same damping. For $\eta = 10^{-6}$, however, 101 radial mesh points are needed to get the damping right and for $\eta = 10^{-7}$ we need $N_\psi \geq 201$. For $\eta = 10^{-8}$ the damping becomes idependent of the spatial resolution for $N_\psi \geq 601$. The oscillatory frequency stays at $Im(\lambda) = 0.58$ and the real part of the frequency converges to $Re(\lambda) = -1.99 \times 10^{-2}$, thus $\delta = 3.4\%$. It is evident that we have a well defined result for $\eta \leq 10^{-6}$.

The gap structure of an equilibrium with $\beta_p = 1\%$ and again $\epsilon^{-1} = 2.5$ is shown in Fig. 12. Except from enlarging the slow- mode continua up to $Im(\lambda) \leq 0.5$ the pressure is not essential — as expected — for the Alfvén branch. Three gaps are present in the shown part of the ideal continuous spectrum : an $m = 1, m = 2$ gap at $q = 3/2$, an $m = 2, m = 3$ gap at $q = 5/2$, and an $m = 1, m = 3$ gap at $q = 2$. There exists a gap mode in this last gap with oscillatory frequency 1.43, which couples to the continuum modes of the $m = 2$ branch that overlays this gap. The corresponding eigenfunction is shown in Fig. 13. The (ideal) singularity is here very pronounced in all five harmonics of the mode because the coupling between the harmonics is stronger now as a consequence of the higher shear and higher pressure as compared to the previous case. The damping too is somewhat higher here : $\delta = 4\%$.

So far the possible strong damping for global toroidal Alfvén waves has been demonstrated. When this mode is excited by energetic particles the absorption of the corresponding energy takes place near the plasma boundary in the two simulations shown so far. It is natural to conjecture that this absorption should also occur near the centre, if the equilbrium profiles are chosen such that a resonance can occur there. An interesting configuration is generated by choosing q on axis as $q_0 = 0.8$ ($q_S = 1.84$) in the previously examined low pressure equilibrium with the density sharply falling at the edge, $D = 0.01$ and $\nu = 2$ in Eq. (8). When the toroidal wave number is $n = -3$ and the poloidal harmonics $m = 1$ to 7 are included, the corresponding toroidal continua yield a wide gap around $s \approx 0.8$ where $q = 1.16$. This gap is generated by the strong coupling of the $m = 3$ and 4 Fourier harmonics. This coupling should take place for $q = -(m + m')/2n = 7/6 = 1.16$, which is indeed confirmed by the results shown in Fig. 14. A global Alfvén mode exists with an eigenvalue $Im(\lambda) \leq 0.96$ well within this gap. This global mode interacts with the

$m = 2$ continuum branch at $s = 0.47$, with the $m = 4$ continuum branch at $s = 0.92$ and with the two $m = 5$ continuum branches at $s = 0.96$ and at $s = 0.97$. The corresponding ideal eigenfunction exhibits a global structure with predominantly $m = 2$, 3 and 4 harmonics and with 4 singular layers at $s = 0.47$ ($m = 2$ branch), at $s = 0.92$ ($m = 4$ branch) and at at $s = 0.96$ and $s = 0.97$ ($m = 5$ branches). Again the singularity of the ideal case $\eta \equiv 0$ is coupled to several Fourier components. In Fig. 15 the radial velocity component of the resistive eigenfunction is shown for $\eta = 10^{-5}$. Here, of course, the singularities have disappeared form the eigenfunction due to the finite conductivity of the plasma. The resistive mode has also a global nature and the ideal singularities are now replaced by a relatively smooth transition in a resistive plasma layer around the ideally singular surfaces. The convergence study for asymptotically small resistivity, shown in Fig. 16, reveals that the damping remains constant for eta smaller than 10^{-6}. Now four basic singularities at four distinct positions have to be resolved accurately. This requires a large number of radial grid points for resolving these four resistive layers in the limit of vanishing resistivity, e.g. up to $N_\psi \geq 801$ for $\eta = 10^{-8}$. Apart from this increased computational effort, the results emerge very clearly. For asymptotically small dissipation the damping becomes independent of dissitation and remains finite, i.e. $\lim_{\eta \to 0} \delta = 9.5\%$. In this case, where resonant absorption takes place at four distinct locations, the damping is indeed large.

5. Conclusions

We have studied the Alfvén spectrum of axisymmetric tokamak plasmas. In contrast to the determination of the continuous part of the ideal MHD spectrum of plasmas with cylinder symmetry, the determination of the ideal continuum of toroidal plasmas is not trivial. The toroidal curvature induces a poloidal mode coupling which is the strongest on rational surfaces where the cylindrical continuum frequencies are at least four-fold degenerate. The effect of the mode coupling is to remove these degeneracies which gives rise to 'avoided crossings' and, by consequence, 'gaps' in the continuous spectrum of finite aspect ratio tokamaks. The size of these gaps is proportional to the strength of the poloidal mode coupling and the appearance of the gaps stresses the importance of two-dimensional effects, e.g. for Alfvén wave heating, since whole frequency bands that yield resonant absorption in one-dimensional (cylindrical) models are not eligible for this heating mechanism in — more realistic — two-dimensional equilibrium models. When the poloidal mode coupling is strong enough, global Alfvén modes are found with a frequency in the above mentioned

gaps. These 'gap modes' might play an important role in controlled thermonuclear fusion as they can be destabilized by interaction with (fusion born) α-particles. These α-particles — whose confinement is essential for ignition and hence for the possibility of generating controlled fusion energy — are lost by particle-wave resonances. However, the interaction of these gap modes with ideal continuum modes causes phase-mixing so that these modes are damped by the same resonant absorption mechanism that enables Alfvén wave heating. The important question now is which of the two phenomena - - destabilization by interaction with α-particles or damping by interaction with continuum modes — is dominant. In the present paper, we were able to quantify the damping of the gap modes due to resonant absorption. The internal structure of the ideal Alfvén continuum is very complex in tokamak plasmas and the gaps that occur at the rational surfaces are 'covered' by one or several continuum branches overlaying the gaps. As a consequence, the gap modes interact with the continuum modes with the same frequency and are damped by phase-mixing. Hence, the gap modes become quasi-modes in ideal MHD. Upon studying these modes in resistive MHD numerically by utilising the code CASTOR, we were able to show that, for asymptotically small resistivity, the damping of the global gap modes is finite and independent of η. We presented cases where the ratio of the real (damping) and imaginary (oscillatory) part of the frequency of the gap modes is of the order of 10% in the ideal-MHD limit.

The existence of TAE modes and their destabilization by neutral beam injection has been demonstrated in TFTR (Wong 1991) and in DIII-D (Heidbrink et al. 1991). In both experiments the pressure due to the energetic particles, β_{hot}, had to exceed the analytic threshold by one order of magnitude in order to produce the predicted instabilities. This clearly indicates that the plasma exhibits a certain damping, most probably in the form of resonant absorption as considered here. A damping in the order of $\delta \approx 0.5 - 1\%$ can easily explain the observed increased threshold for β_{hot}. Further detailed studies have to be performed to show whether the damping can yield indeed re-absorption of the energy near the plasma center and whether the high damping rates with $\delta \approx 5 - 10\%$ can be realised by appropriately modifying the density profiles. In this context, experiments with pellet injection are of great interest.

Acknowledgements

This work was supported by the European Community Scientific Cooperation un-

der grant Nr. SC1-0255-C. S. Poedts was supported by a scientific and technical grant awarded by the Commission of the European Communities, Directorate-General for Science, Research and Development (DG XII-JRC). We thank M. Goossens, G. Halberstadt, R.A.M. Van der Linden, and H. Weitzner for stimulating discussions and suggestions.

References

Berk, H.L., van Dam, J.W., Guo, Z., and Lindberg, D.M. : 'Continuum Damping of Toroidicity-induced Shear Alfvén Eigenmodes', IFS Report **499** (September 1990).

Cheng, C.Z. : *Phys. Fluids B*, **2**, 1427 (1990).

Cheng, C.Z. : *Phys. Fluids B*, **3**, 2463 (1991).

Cheng, C.Z., and Chance, M.S. : *Phys. Fluids* **29**, 3695 (1986).

Fu, G.Y. and van Dam, J.W. : *Phys. Fluids B*, **1**, 1949 (1989a).

Fu, G.Y. and van Dam, J.W. : *Phys. Fluids B*, **1**, 2404 (1989b).

Goedbloed, J.P. : *Phys. Fluids* **18**, 1258 (1975).

Goedbloed, J.P. : *Physica*, **12D**, 107 (1984).

Goedbloed, J.P. : Trends in Physics, Proc. of the 8th General Conference of the European Physycal Society, Sept. 4–6, 1990, 827 (1991).

Heidbrink, W.W., Strait, E.J., Doyle, E., Sager, G., and Snider, R. : 'An Investigation of Beam-Driven Alfvén Instabilities in the DIII-D Tokamak', submitted to Nucl. Fusion.

Huysmans, G.T.A., Goedbloed, J.P., and Kerner, W. : *Europhysics 2nd Int. Conf. on Computational Physics*, Amsterdam, 1990, CP90, Ed. A. Tenner, World Scientific Signapore, 371 (1991).

Kerner, W., Poedts, S., Goedbloed, J.P., Huysmans, G.T.A., Keegan, B., Schwarz, E. : '*Proc. of 18th European Conference on Controlled Fusion and Plasma Physics*, Berlin,

June 3–7, IV.89–IV.92 (1991).

Pao, Y.-P. : *Nucl. Fusion* **15**, 631 (1975).

Poedts, S. Kerner, W., and Goossens, M. : *J. Plasma Physics* **42**, 27 (1989).

Poedts, S., and Kerner, W. : *Phys. Rev. Letters*, **66**, 2871–2874 (1991).

Poedts, S., and Schwarz, E. : *J. Comp. Physics*, submitted.

Porcelli, F. : *Plasma Phys. and Contr. Fusion*, **33**, 1601 (1991).

Rosenbluth, M.N., Berk, H.L., van Dam, J.W., and Lindberg, D.M. : 'Asymptotic Theory of Toroidal Alfvén Eigenmodes in Ignited Tokamaks', IFS Report **518** (August 1991).

Wong, K.L. : *Phys. Rev. Letters*, **66**, 1874 (1991).

Zorca, F. and Chen, L. : *Bull. Am. Phys. Soc.*, **35**, 2069 (1990).

Figure captions

Figure 1 : a) The ideal MHD continuous spectrum, in particular local Alfvén and slow magnetosonic frequencies versus s for a circular cross- section toroidal plasma with $\epsilon = 0.4$, $q_0 = 1.10$, $q_S = 2.66$, and $\beta_p \approx 2\%$. The density varies according to Eq. (8) with $D = 0.5$ and $\nu = 2$. The wave numbers are chosen as $n = -1$, and m = 0,1,2,3, and 4. b) Corresponding part of the full ideal MHD spectrum as obtained by using CASTOR ($N_\psi = 21$, same wave numbers). Within the numerical accuracy the real part of λ is zero ($\eta = 0$).

Figure 2 : Radial dependence of the Fourier harmonics of the rv_r- component of the eigenfunction of the discrete Alfvén mode with a frequency located in the basic gap shown in Fig. 1 (as indicated in Fig. 1b).

Figure 3 : Relative distance of the frequency of the gap mode from the lower edge of the gap versus the (poloidal) plasma beta. Here $\epsilon = 0.4$, $q_0 = 1.2$, $D = 0.01$, $\nu = 2$, $n = -1$, and m =0, 1, 2, 3, and 4.

Figure 4 : Width of the basic ($m = 1$ and 2) gap and frequencies of discrete gap modes therein versus the inverse aspect ratio. The other parameters are chosen as $q_0 = 1.05$, $D = 0.5$, $\nu = 2$, $n = -1$, and m =0, 1, 2, 3, and 4.

Figure 5 : Radial dependence of the dominant Fourier harmonics of the rv_r-component of the eigenfunction of the second gap mode with $Im(\lambda) = 0.80$ as indicated in Fig. 4 for $\epsilon = 0.8$.

Figure 6 : a) Structure of the ideal-MHD continuous spectrum for $n = -3$ and m =2, 3, 4, 5, and 6, $q = 1.05$ and a density profile given by Eq. 8 with $D = 0.05$ and $\nu = 1$. b) Corresponding part of the full ideal-MHD spectrum obtained by using CASTOR. Because of the coarse grid ($N_\psi = 21$) the singularity in the gap modes is not resolved and the real part of λ is found to be zero. The correct damping can be determined by means of a convergence study as shown in Section 4.

Figure 7 : Radial dependence of the Fourier harmonics of the real part of the rv_r-components of the two gap modes with a) $Im(\lambda) = 0.46$ and b) $Im(\lambda) = 0.53$ as indicated in Fig. 6b.

Figure 8 : Structure of the ideal-MHD continuous spectrum for $n = -5$ and $m = 3 \rightarrow 13$, $q_0 = 1.05$ and a density profile given by Eq. 8 with $D = 0.1$ and $\nu = 1$.

Figure 9 : Structure of the ideal-MHD continuous spectrum for $n = -1$ and $m = 0 \rightarrow 4$, $q_0 = 1.10$ and a density profile given by Eq. 8 with $D = 0.01$ and $\nu = 2$.

Figure 10 : Radial dependence of the Fourier harmonics of the real part of the rv_r-component of the gap mode with the frequency $Im(\lambda) = 0.58$ as indicated in Fig. 9 a) for $\eta = 0$ and $N_\psi = 401$ and b) for $\eta = 10^{-7}$ and $N_\psi = 401$. The other parameters are chosen as in Fig. 9.

Figure 11 : Relative damping versus plasma resistivity for the mode shown in Fig. 10 and for different values of N_ψ. This convergence study shows the need for a sufficiently high resolution in the resistive layer in order to get the damping correct.

Figure 12 : Structure of the ideal-MHD continuous spectrum of a higher- pressure tokamak plasma with $\epsilon^{-1} = 2.5$ and $\beta_p = 0.31$, for $n = -1$ and $m = 1 \rightarrow 5$, $q_0 = 1.05$ and a density profile given by Eq. 8 with $D = 0.05$ and $\nu = 1$.

Figure 13 : Radial dependence of the Fourier harmonics of the real part of the rv_r-component of the gap mode with the frequency $Im(\lambda) = 1.44$ as indicated in Fig. 12 for $\eta = 0$ and $N_\psi = 301$.

Figure 14 : Structure of the ideal-MHD continuous spectrum for $n = -3$ and $m = 1 \rightarrow 7$, $q_0 = 0.8$ and a density profile given by Eq. 8 with $D = 0.01$ and $\nu = 2$.

Figure 15 : Radial dependence of the Fourier harmonics of the real part of the rv_r-component of the gap mode with the frequency $Im(\lambda) = 0.96$ as indicated in Fig. 14 for $\eta = 10^{-5}$ and $N_\psi = 201$.

Figure 16 : Relative damping versus plasma resistivity for the mode shown in Fig. 15 and for different values of N_ψ again showing the need for a sufficiently high resolution in the resistive layer in order to get the damping correct.

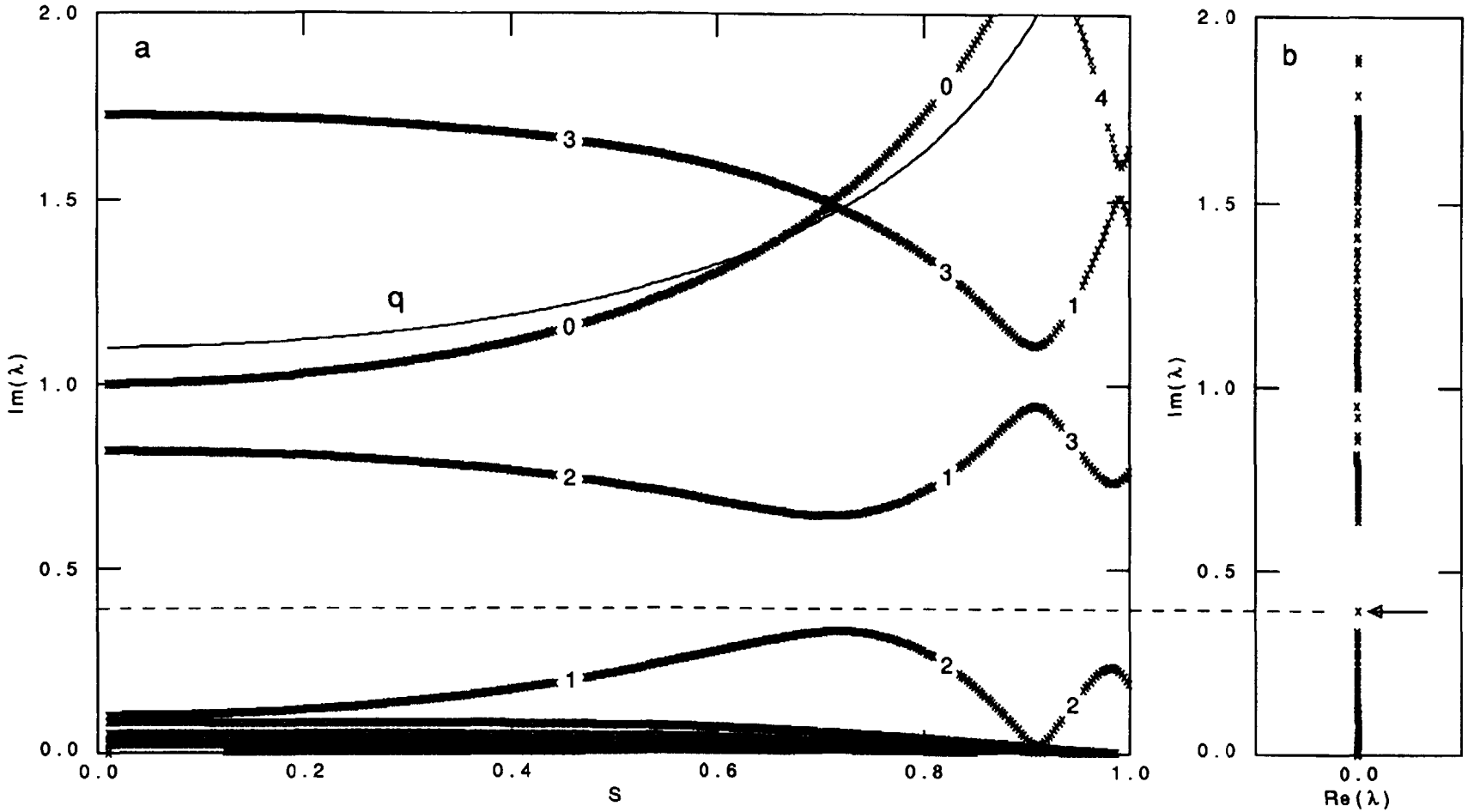

Figure 1

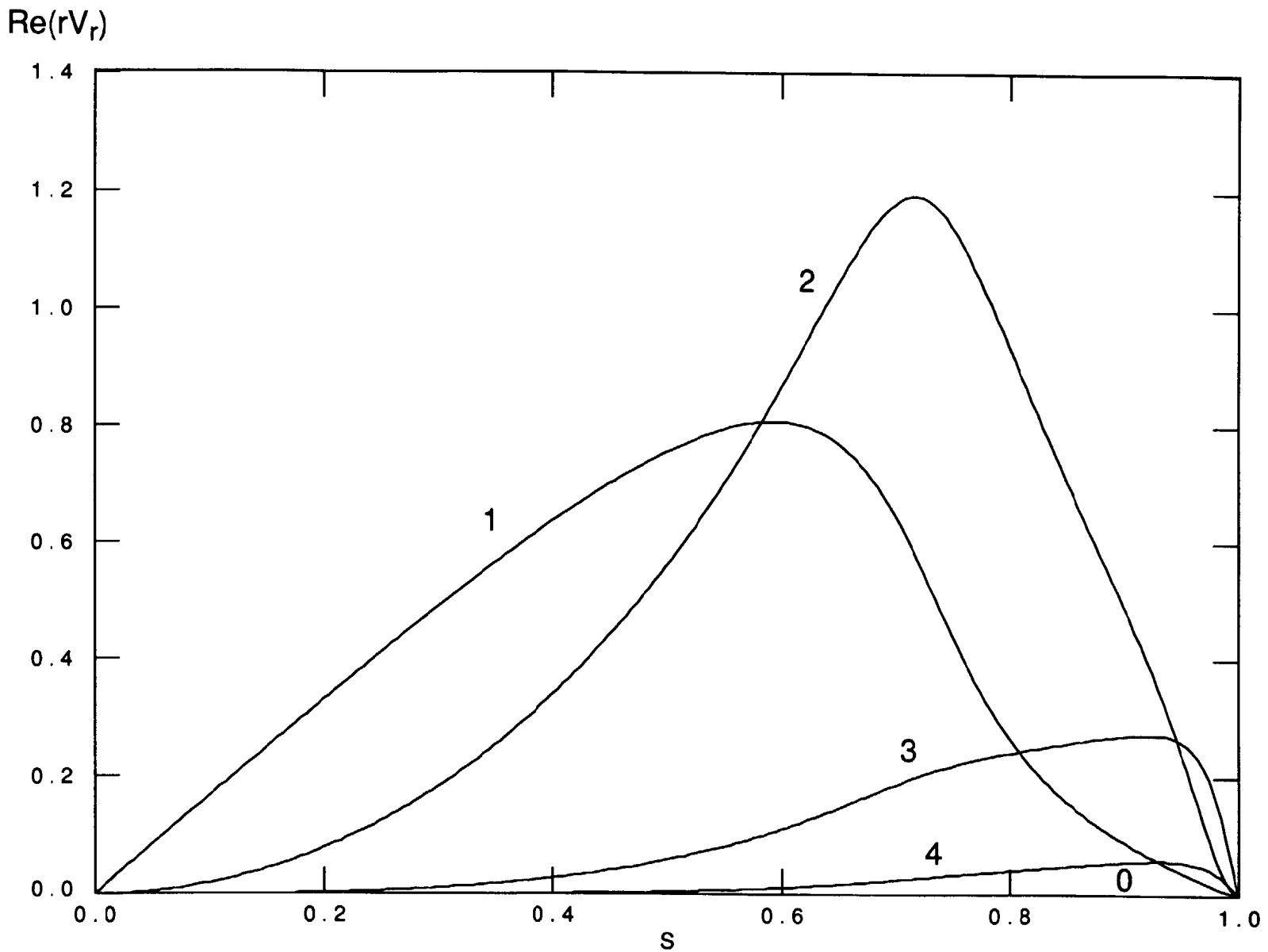

Figure 2

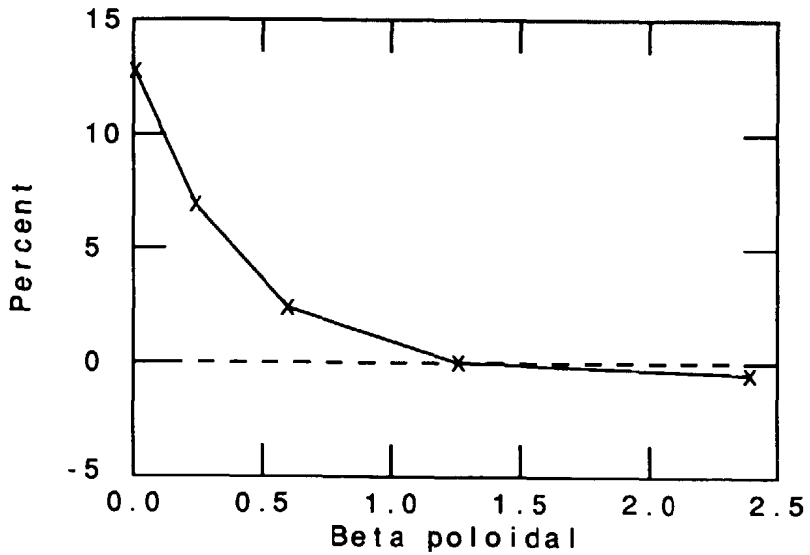

Figure 3

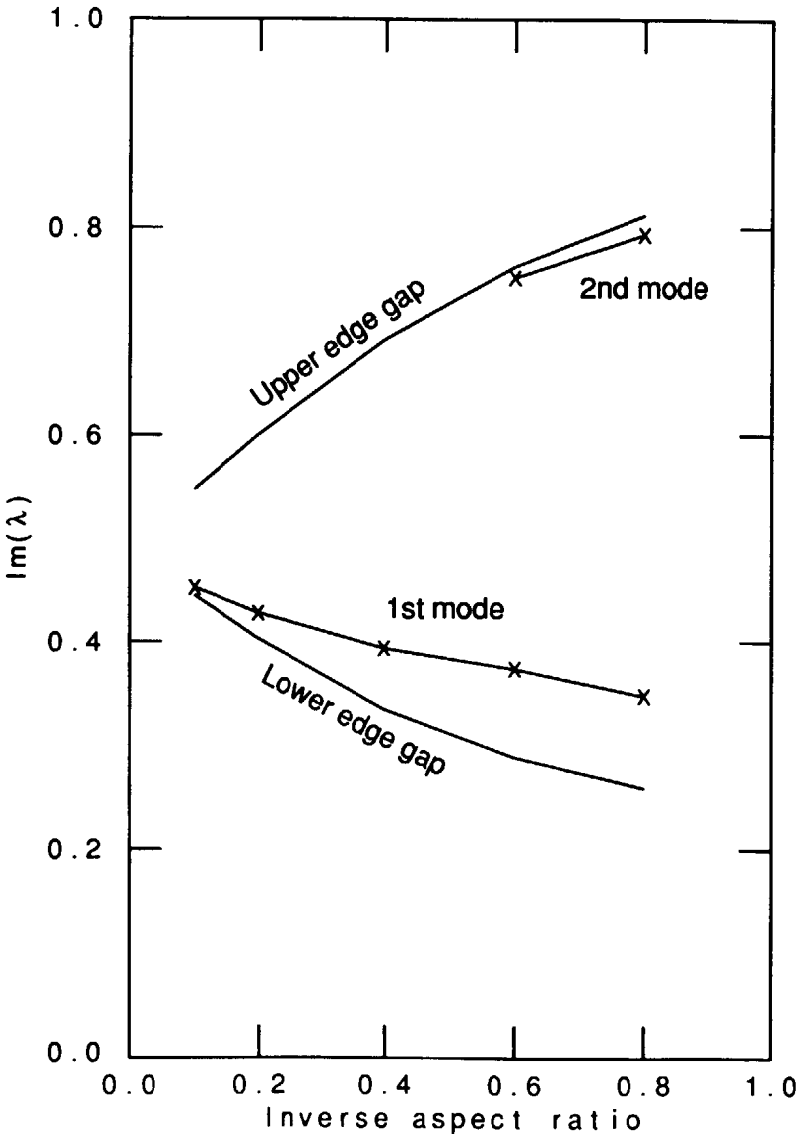
1.0
0.8
0.6
0.4
0.2
0.0
Im(λ)
Upper edge gap
2nd mode
1st mode
Lower edge gap
0.0
0.2
0.4
0.6
0.8
1.0
Inverse aspect ratio

Figure 4

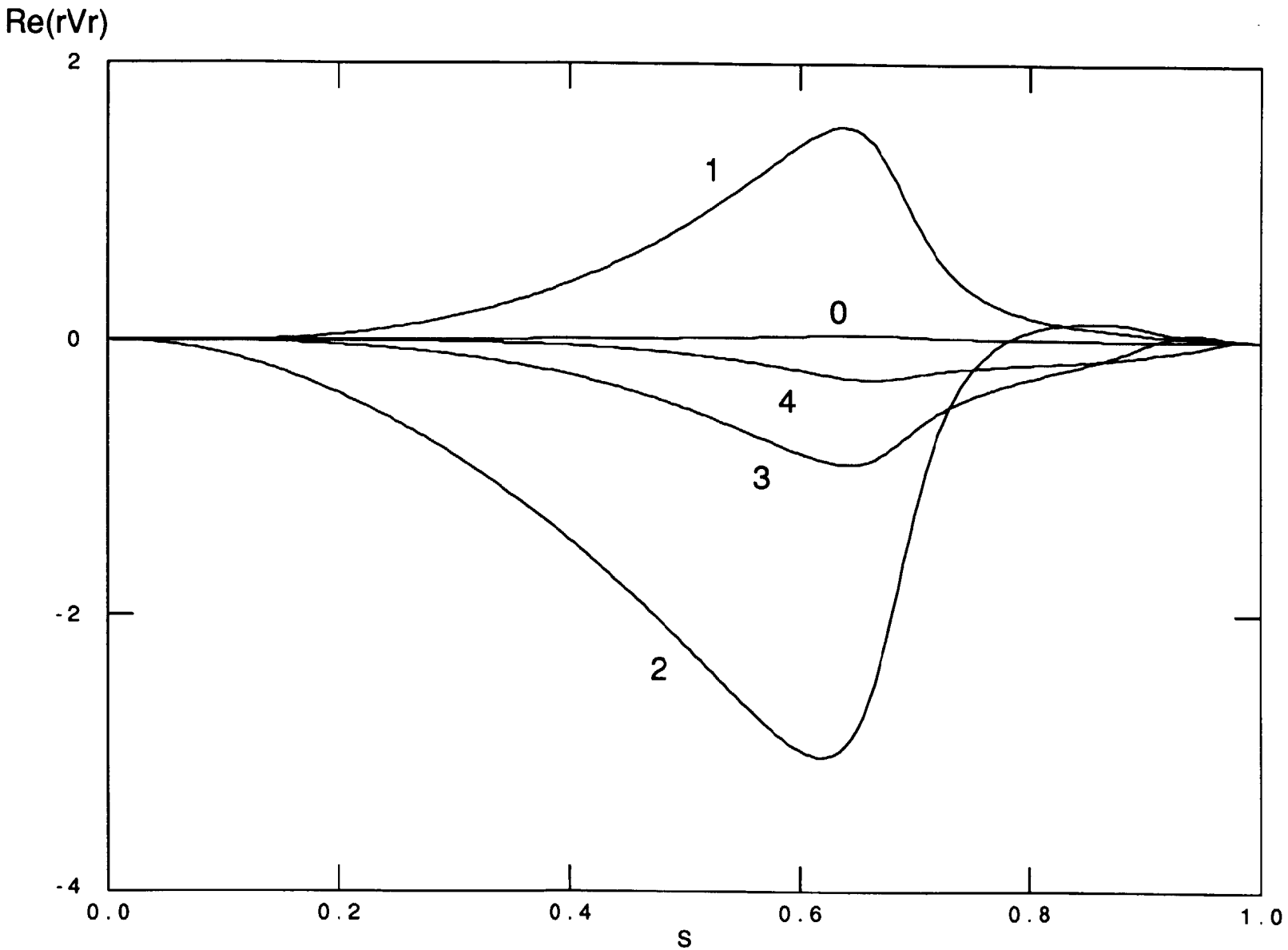

Figure 5

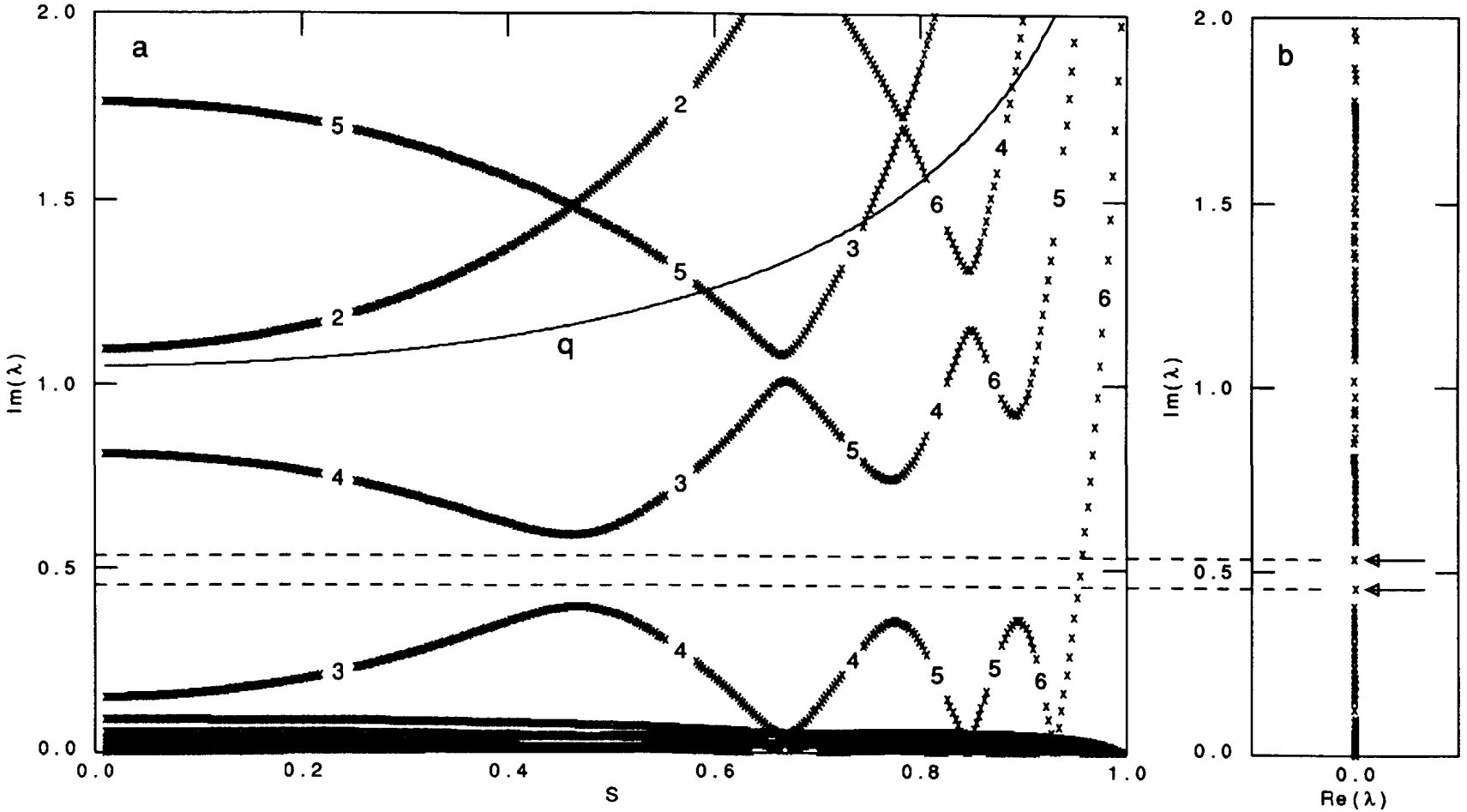

Figure 6

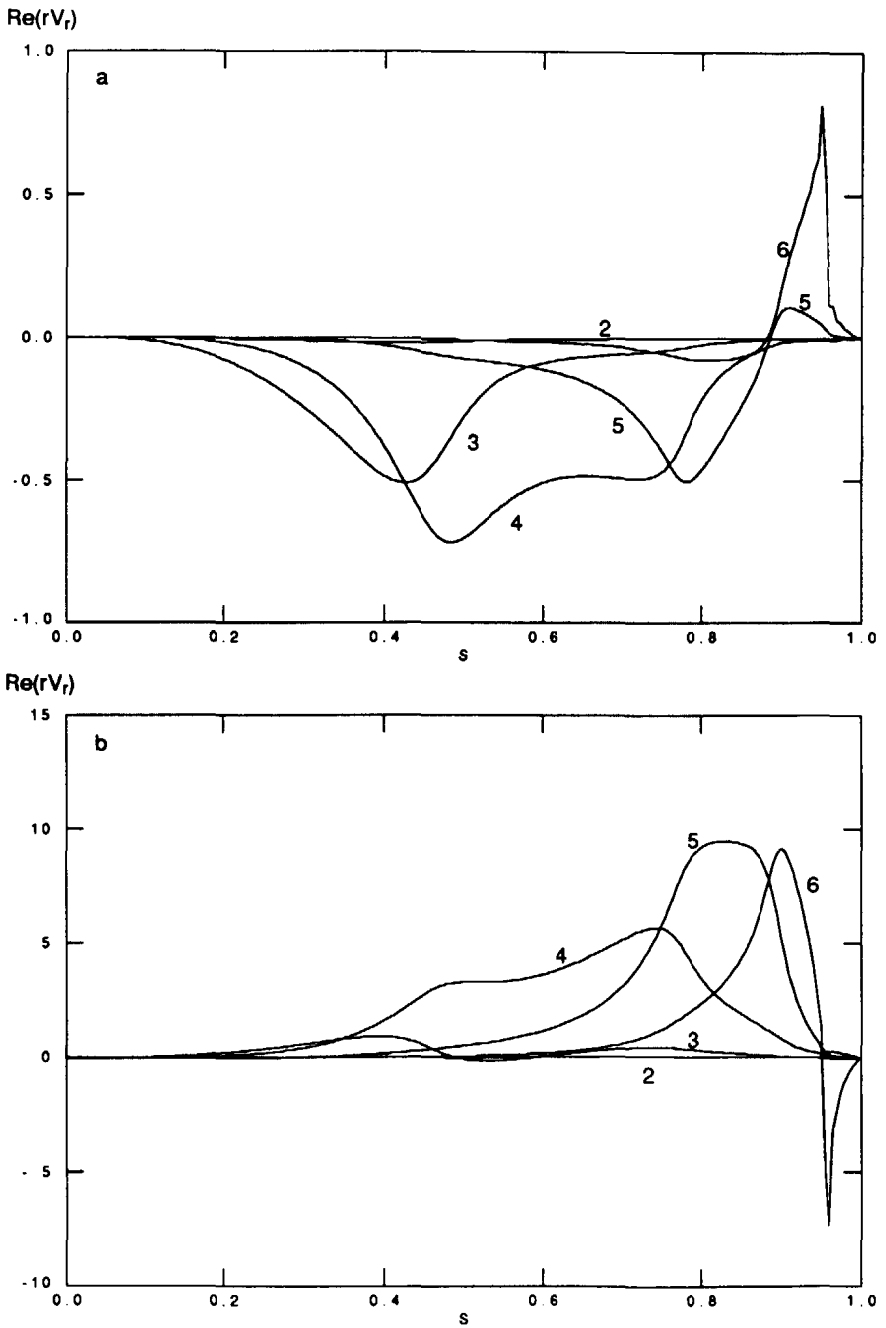
Re(rV_r)
a
1.0
0.5
0.0
-0.5
-1.0
0.0
0.2
0.4
0.6
0.8
1.0
s
2
3
4
5
6
Re(rV_r)
b
15
10
5
0
-5
-10
0.0
0.2
0.4
0.6
0.8
1.0
s
2
3
4
5
6

Figure 7

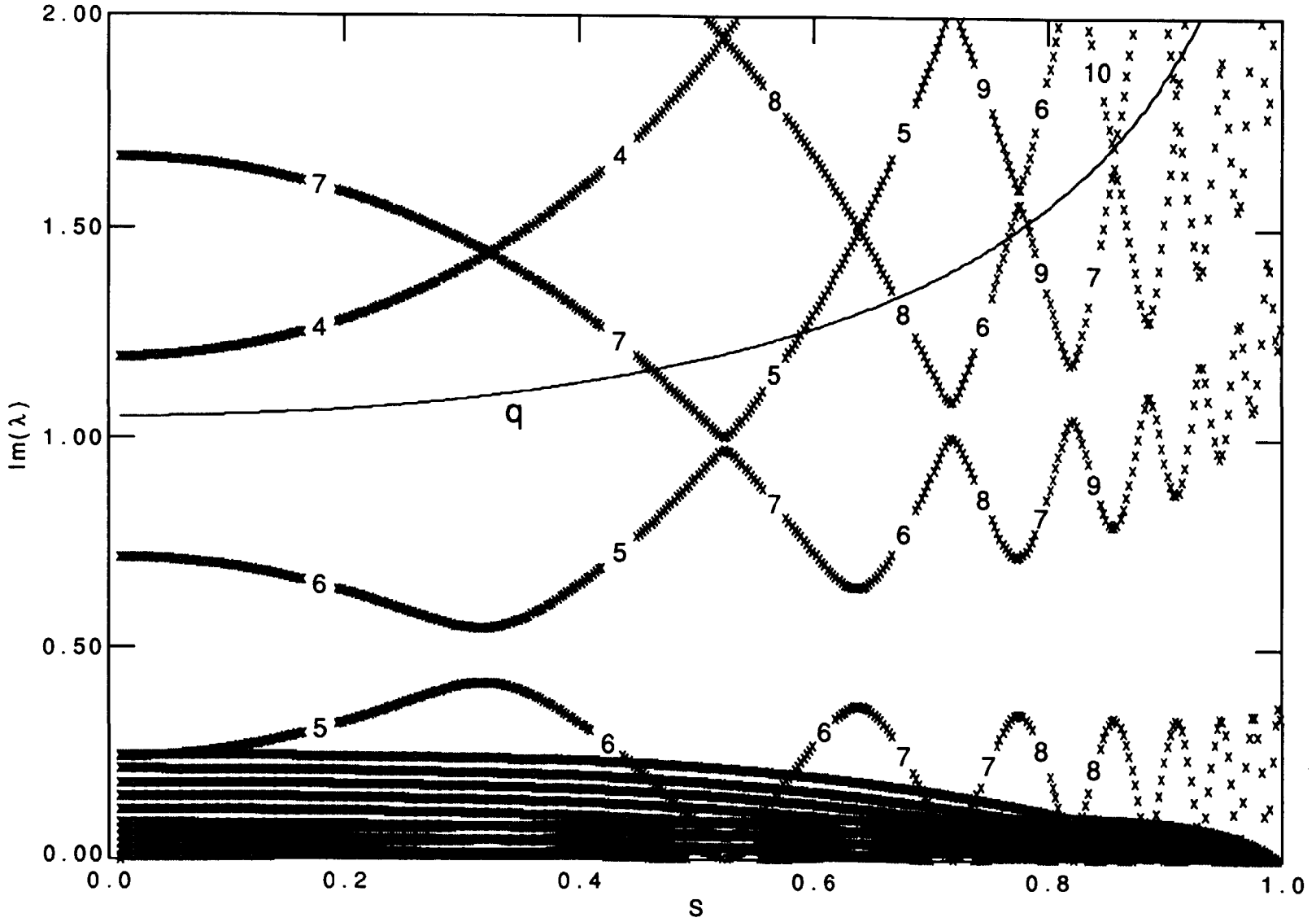

Figure 8

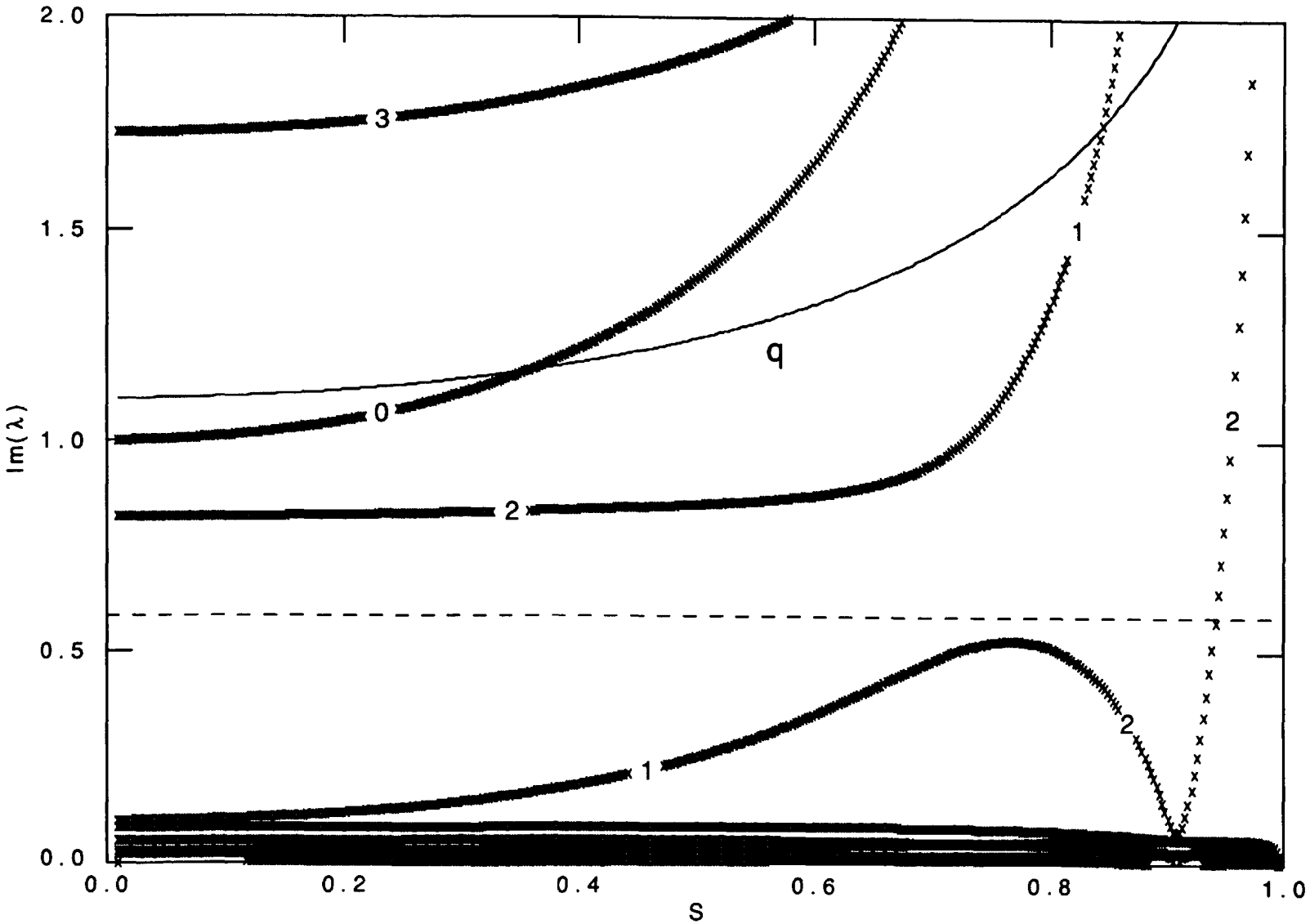

Figure 9

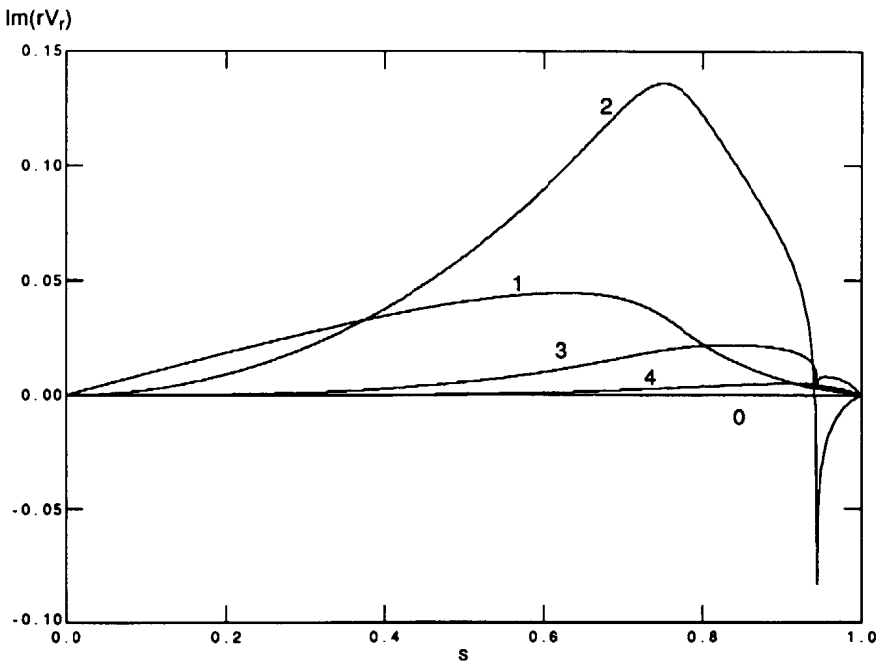
Im(rV_r)
0.15
0.10
0.05
0.00
-0.05
-0.10
0.0
0.2
0.4
0.6
0.8
1.0
s
2
1
3
4
0

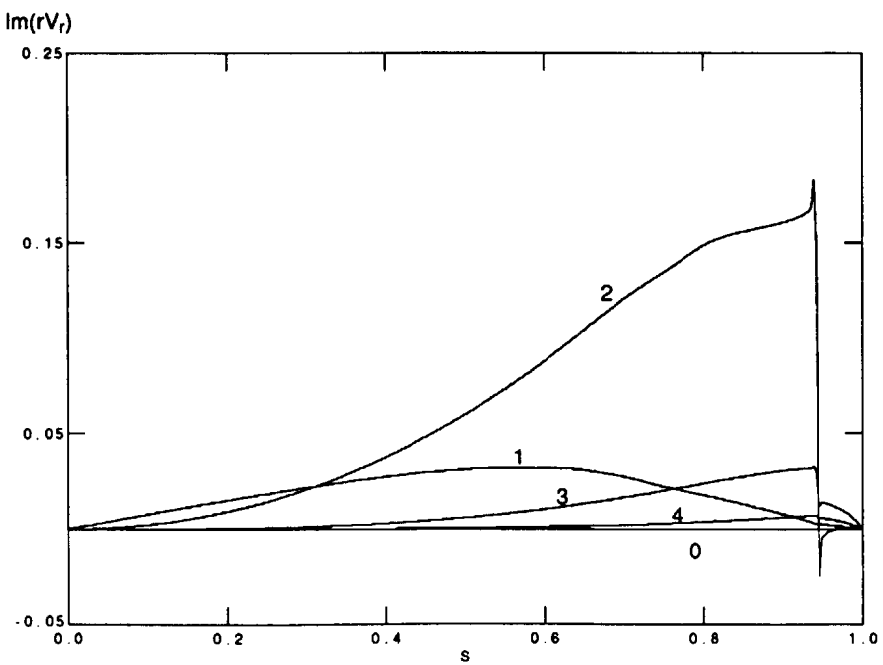
Im(rV_r)
0.25
0.15
0.05
-0.05
0.0
0.2
0.4
0.6
0.8
1.0
s
2
1
3
4
0

Figure 10

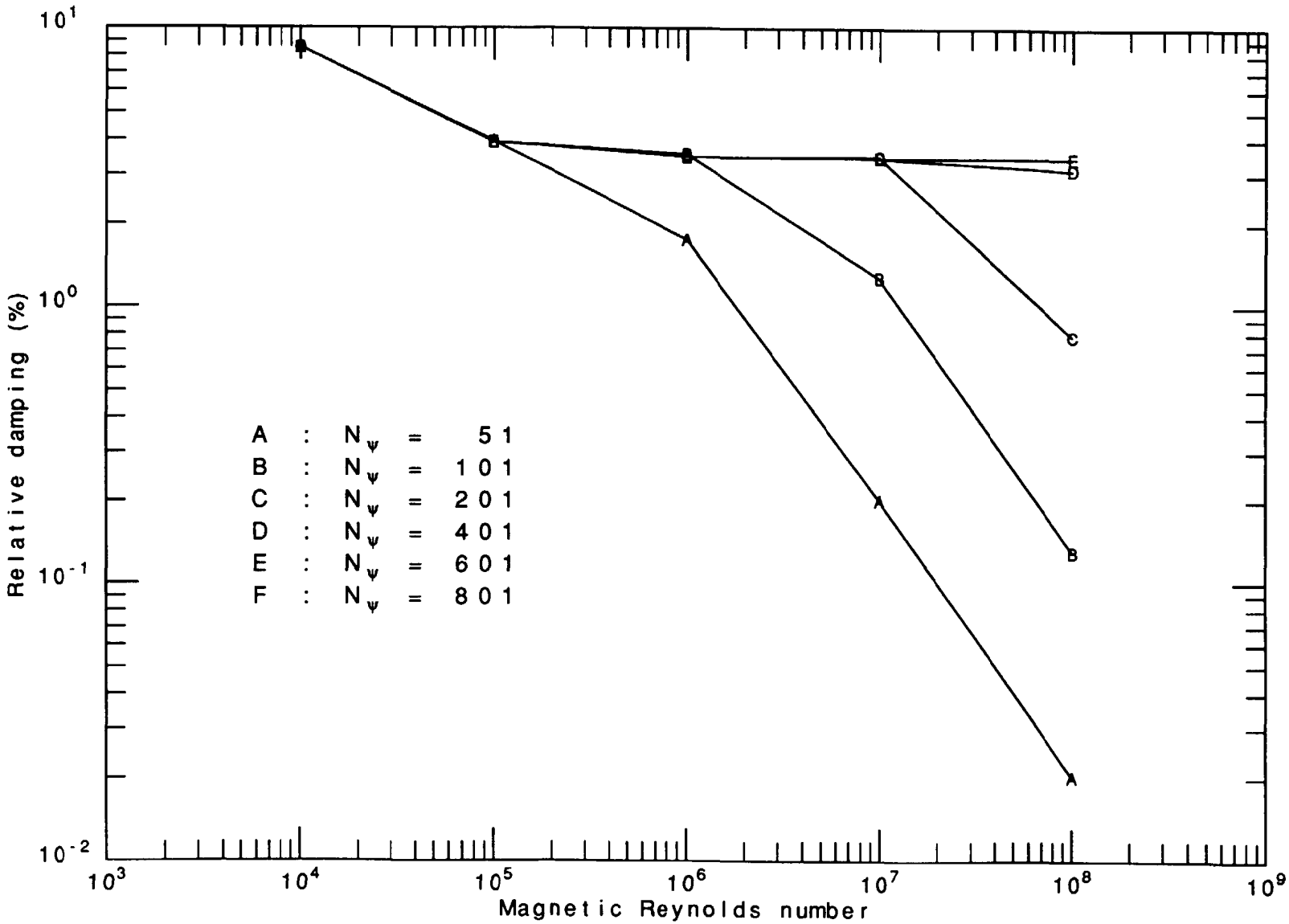
Relative damping (%)
10^{1}
10^{0}
10^{-1}
10^{-2}
A : N_ψ = 51
B : N_ψ = 101
C : N_ψ = 201
D : N_ψ = 401
E : N_ψ = 601
F : N_ψ = 801
10^{3}
10^{4}
10^{5}
10^{6}
10^{7}
10^{8}
10^{9}
Magnetic Reynolds number

Figure 11

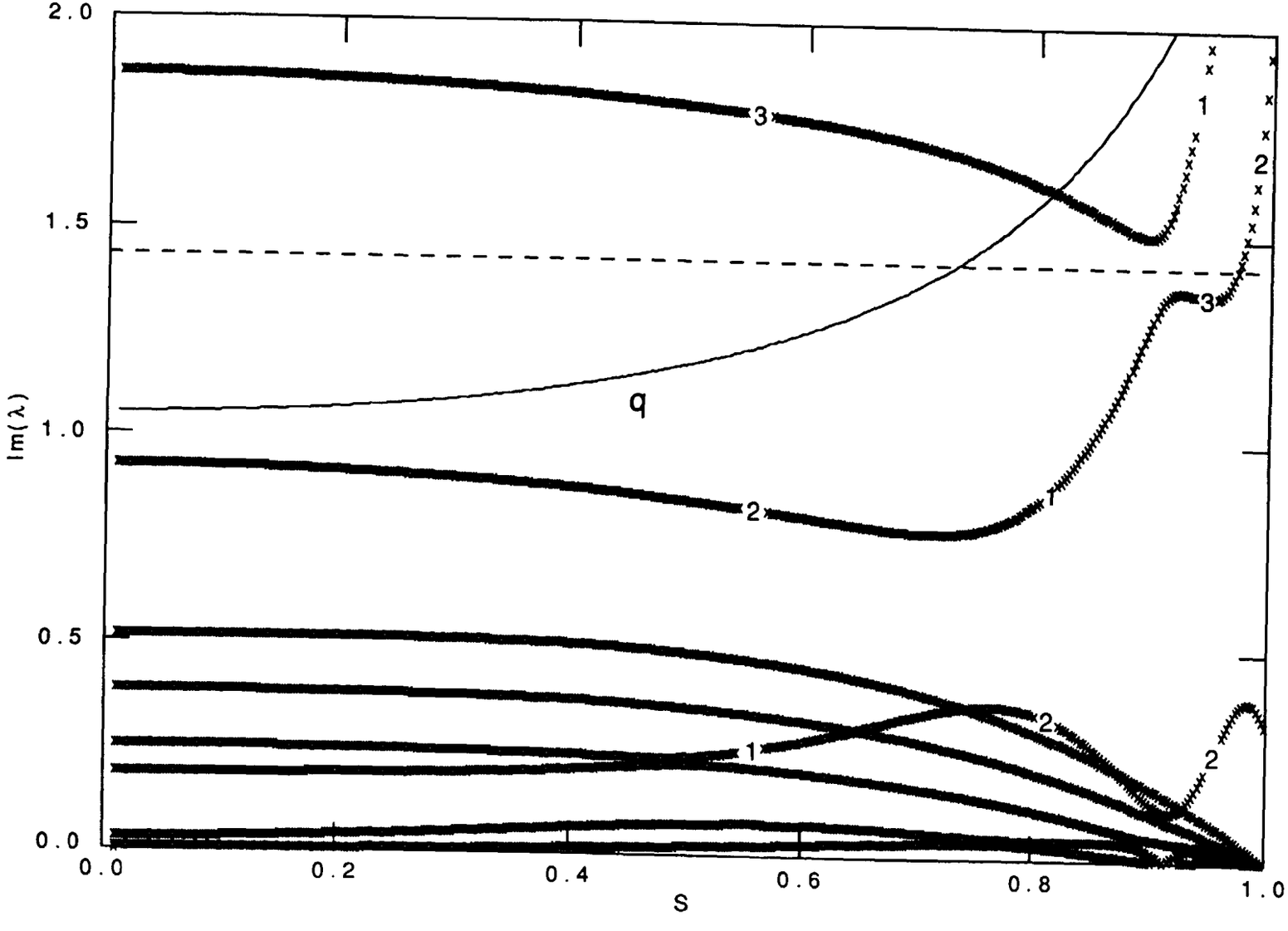

Figure 12

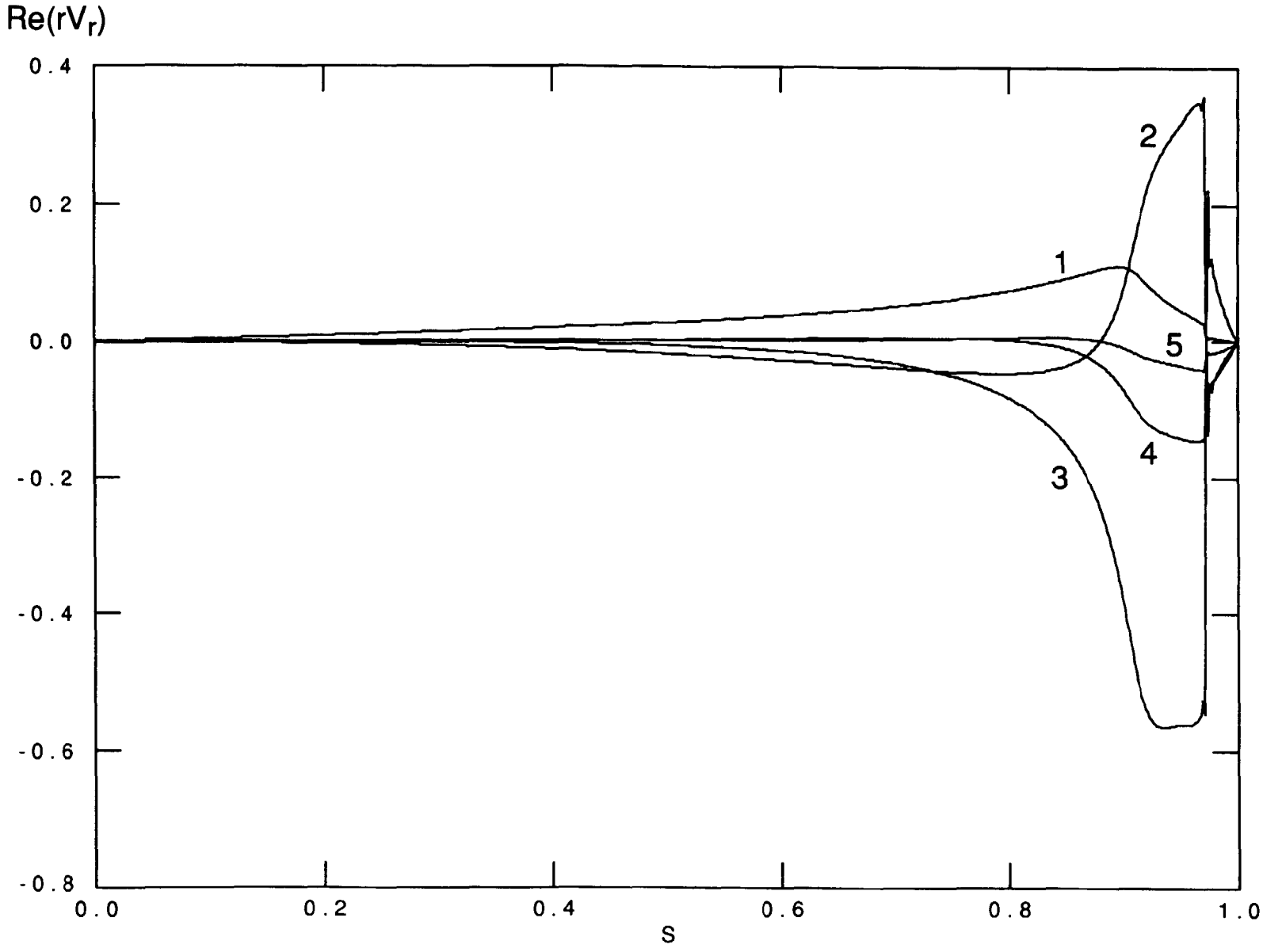

Figure 13

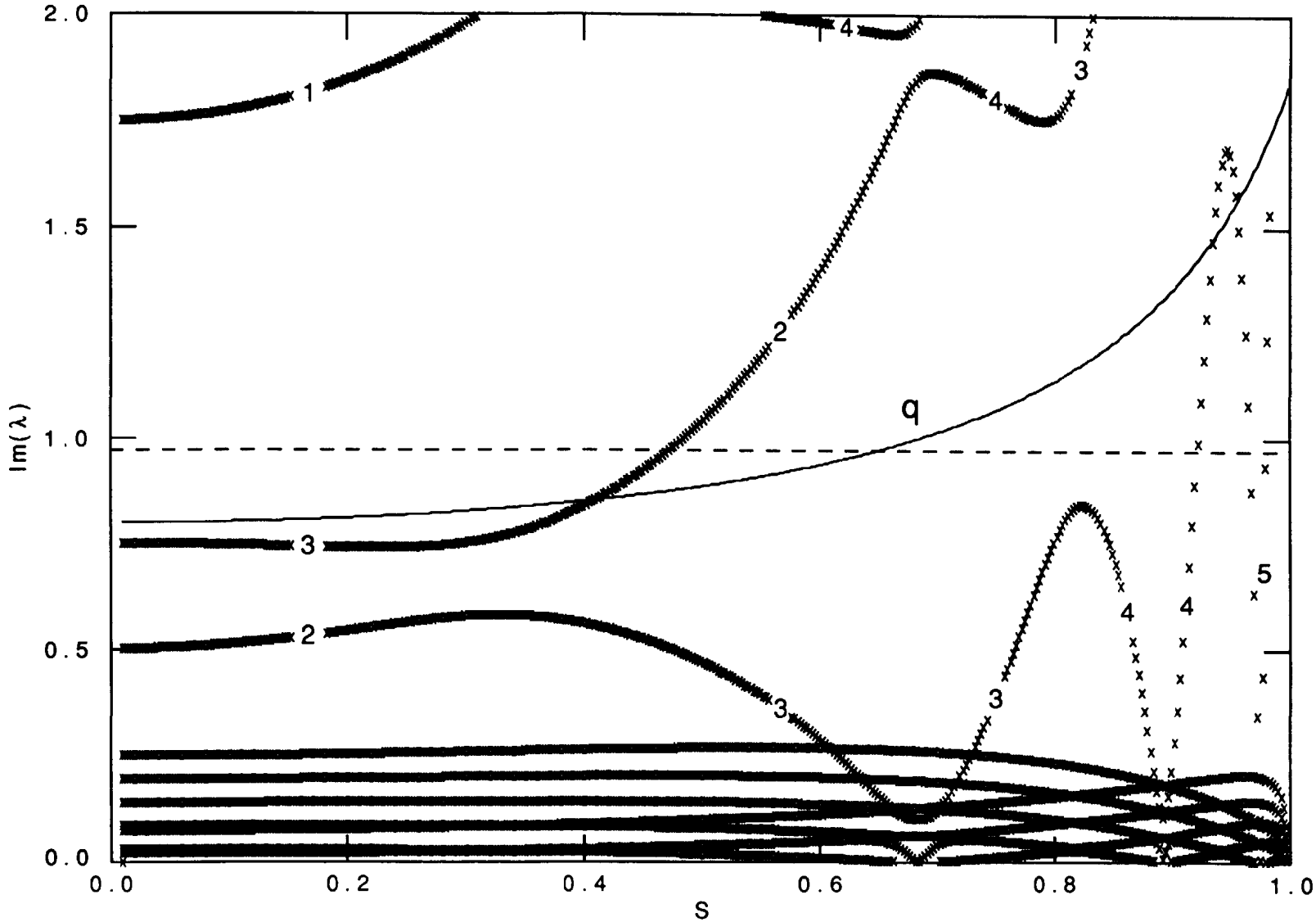

Figure 14

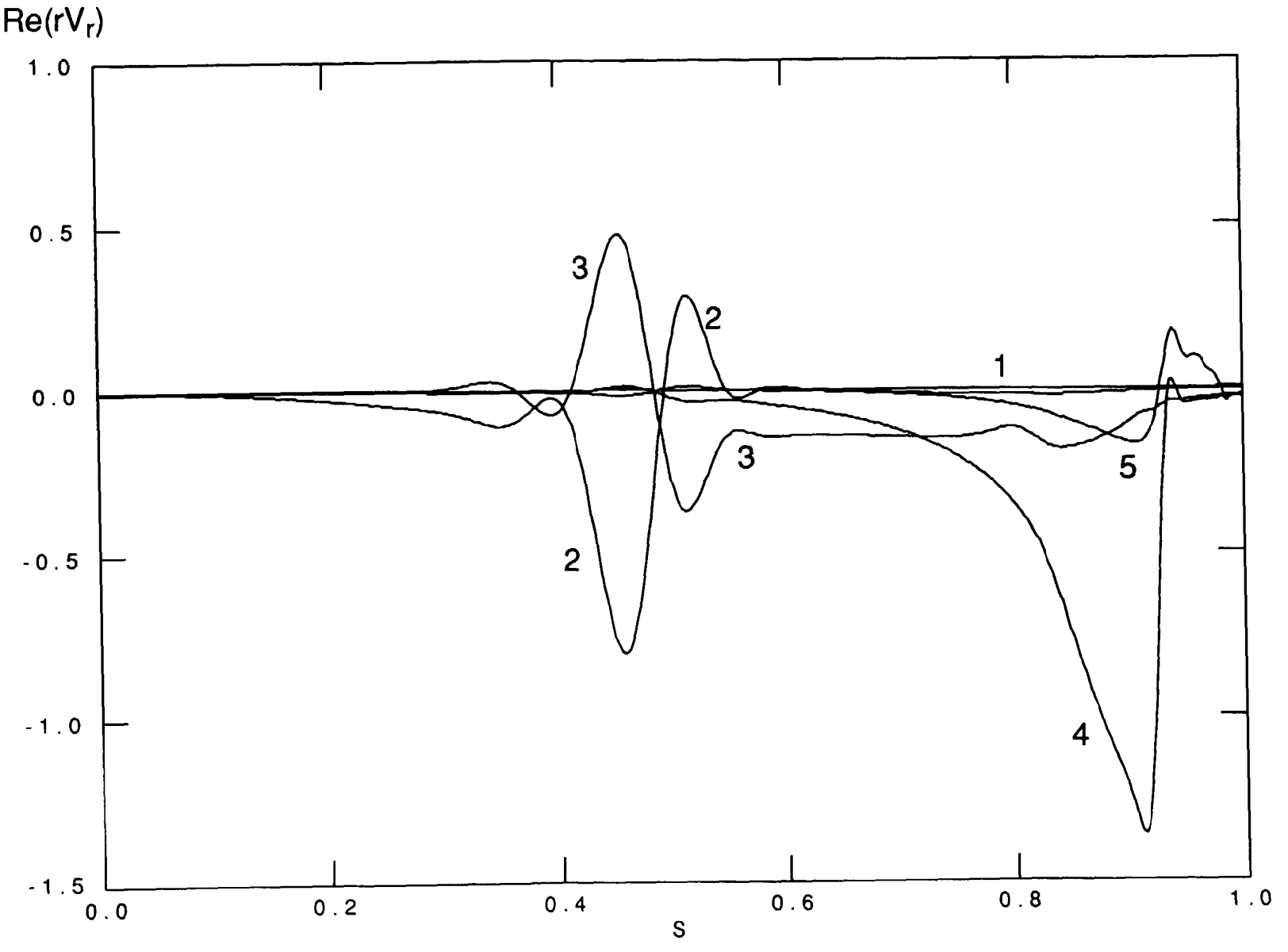

Figure 15

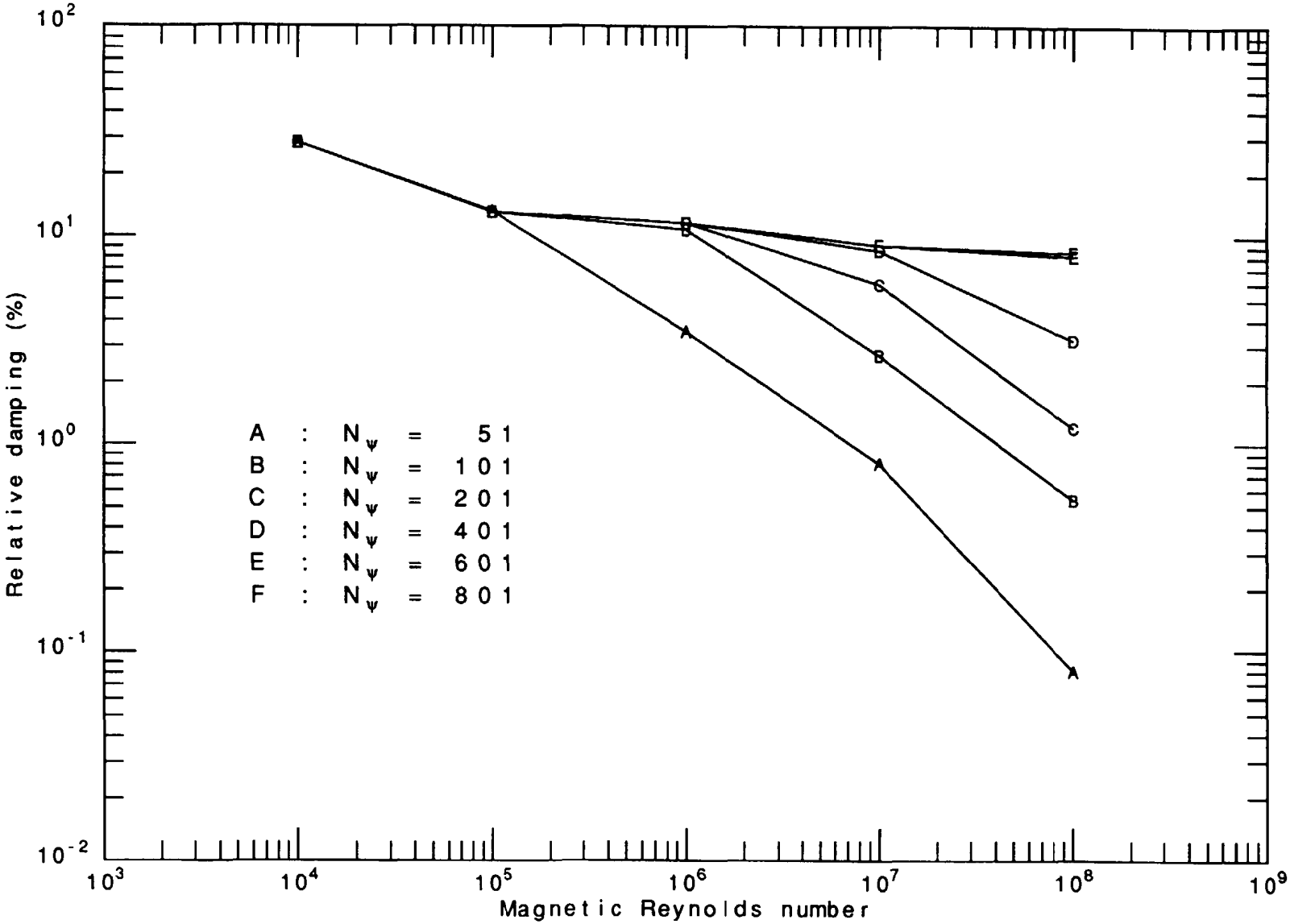
Relative damping (%)
10^2
10^1
10^0
10^{-1}
10^{-2}
10^3
10^4
10^5
10^6
10^7
10^8
10^9
Magnetic Reynolds number
A : N_ψ = 51
B : N_ψ = 101
C : N_ψ = 201
D : N_ψ = 401
E : N_ψ = 601
F : N_ψ = 801

Figure 16

ANNEX

P.-H. REBUT, A. GIBSON, M. HUGUET, J.M. ADAMS[1], B. ALPER, H. ALTMANN, A. ANDERSEN[2], P. ANDREW[3], M. ANGELONE[4], S. ALI-ARSHAD, P. BAIGGER, W. BAILEY, B. BALET, P. BARABASCHI, P. BARKER, R. BARNSLEY[5], M. BARONIAN, D.V. BARTLETT, L. BAYLOR[6], A.C. BELL, G. BENALI, P. BERTOLDI, E. BERTOLINI, V. BHATNAGAR, A.J. BICKLEY, D. BINDER, H. BINDSLEV[2], T. BONICELLI, S.J. BOOTH, G. BOSIA, M. BOTMAN, D. BOUCHER, P. BOUCQUEY, P. BREGER, H. BRELEN, H. BRINKSCHULTE, D. BROOKS, A. BROWN, T. BROWN, M. BRUSATI, S. BRYAN, J. BRZOZOWSKI[7], R. BUCHSE[22], T. BUDD, M. BURES, T. BUSINARO, P. BUTCHER, H. BUTTGEREIT, C. CALDWELL-NICHOLS, D.J. CAMPBELL, P. CARD, G. CELENTANO, C.D. CHALLIS, A.V. CHANKIN[8], A. CHERUBINI, D. CHIRON, J. CHRISTIANSEN, P. CHUILON, R. CLAESEN, S. CLEMENT, E. CLIPSHAM, J.P. COAD, I.H. COFFEY[9], A. COLTON, M. COMISKEY[10], S. CONROY, M. COOKE, D. COOPER, S. COOPER, J.G. CORDEY, W. CORE, G. CORRIGAN, S. CORTI, A.E. COSTLEY, G. COTTRELL, M. COX[11], P. CRIPWELL[12], O. Da COSTA, J. DAVIES, N. DAVIES, H. de BLANK, H. de ESCH, L. de KOCK, E. DEKSNIS, F. DELVART, G.B. DENNE-HINNOV, G. DESCHAMPS, W.J. DICKSON[13], K.J. DIETZ, S.L. DMITRENKO, M. DMITRIEVA[14], J. DOBBING, A. DOGLIO, N. DOLGETTA, S.E. DORLING. P.G. DOYLE, D.F. DÜCHS, H. DUQUENOY, A. EDWARDS, J. EHRENBERG, A. EKEDAHL, T. ELEVANT[7], S.K. ERENTS[11], L.G. ERIKSSON, H. FAJEMIROKUN[12], H. FALTER, J. FREILING[15], F. FREVILLE, C. FROGER, P. FROISSARD, K. FULLARD, M. GADEBERG, A. GALETSAS, T. GALLAGHER, D. GAMBIER, M. GARRIBBA, P. GAZE, R. GIANNELLA, R.D. GILL, A GIRARD, A. GONDHALEKAR, D. GOODALL[11], C. GORMEZANO, N.A. GOTTARDI, C. GOWERS, B.J. GREEN, B. GRIEVSON, R. HAANGE, A. HAIGH, C.J. HANCOCK, P.J. HARBOUR, T. HARTRAMPF, N.C. HAWKES[11], P. HAYNES[11], J.L. HEMMERICH, T. HENDER[11], J. HOEKZEMA, D. HOLLAND, M. HONE, L. HORTON, J. HOW, M. HUART, I. HUGHES, T.P. HUGHES[10], M. HUGON, Y. HUO[16], K. IDA[17], B. INGRAM, M. IRVING, J. JACQUINOT, H. JAECKEL, J.F. JAEGER, G. JANESCHITZ, Z. JANKOVICZ[18], O.N. JARVIS, F. JENSEN, E.M. JONES, H.D. JONES, L.P.D.F. JONES, S. JONES[19], T.T.C. JONES, J.-F. JUNGER, F. JUNIQUE, A. KAYE, B.E. KEEN, M. KEILHACKER, G.J. KELLY, W. KERNER, A. KHUDOLEEV[21], R. KONIG, A. KONSTANTELLOS, M. KOVANEN[20], G. KRAMER[15], P. KUPSCHUS, R. LÄSSER, J.R. LAST, B. LAUNDY, L. LAURO-TARONI, M. LAVEYRY, K. LAWSON[11], M. LENNHOLM, J. LINGERTAT[22], R.N. LITUNOVSKI, A. LOARTE, R. LOBEL, P. LOMAS, M. LOUGHLIN, C. LOWRY, J. LUPO, A.C. MAAS[15], J. MACHUZAK[19], B. MACKLIN, G. MADDISON[11], C.F. MAGGI[23], G. MAGYAR, W. MANDL[22], V. MARCHESE, G. MARCON, F. MARCUS, J. MART, D. MARTIN, E. MARTIN, R. MARTIN-SOLIS[24], P. MASSMANN, G. MATTHEWS, H. McBRYAN, G. McCRACKEN[11], J. McKIVITT, P. MERIGUET, P. MIELE, A. MILLER, J. MILLS, S.F. MILLS, P. MILLWARD, P. MILVERTON, E. MINARDI[4], R. MOHANTI[25], P.L. MONDINO, D. MONTGOMERY[26], A. MONTVAI[27], P. MORGAN, H. MORSI, D. MUIR, G. MURPHY, R. MYRNÄS[28], F. NAVE[29], G. NEWBERT, M. NEWMAN, P. NIELSEN, P. NOLL, W. OBERT, D. O'BRIEN, J. ORCHARD, J. O'ROURKE, R. OSTROM, M. OTTAVIANI, M. PAIN, F. PAOLETTI, S. PAPASTERGIOU, W. PARSONS, D. PASINI, D. PATEL, A. PEACOCK, N. PEACOCK[11], R.J.M. PEARCE, D. PEARSON[12], J.F. PENG[16], R. PEPE DE SILVA, G. PERINIC, C. PERRY, M. PETROV[21], M.A. PICK, J. PLANCOULAINE, J.-P POFFÉ, R. PÖHLCHEN, F. PORCELLI, L. PORTE[13], R. PRENTICE, S. PUPPIN, S. PUTVINSKII[8], G. RADFORD[30], T. RAIMONDI, M.C. RAMOS DE ANDRADE, R. REICHLE, J. REID, S. RICHARDS, E. RIGHI, F. RIMINI, D. ROBINSON[11], A. ROLFE, R.T. ROSS, L. ROSSI, R. RUSS, P. RUTTER, H.C. SACK, G. SADLER, G. SAIBENE, J.L. SALANAVE, G. SANAZZARO, A. SANTAGIUSTINA, R. SARTORI, C. SBORCHIA, P. SCHILD, M. SCHMID, G. SCHMIDT[31], B. SCHUNKE, S.M. SCOTT, L. SERIO, A SIBLEY, R. SIMONINI, A.C.C. SIPS, P. SMEULDERS, R. SMITH, R. STAGG, M. STAMP, P. STANGEBY[3], R. STANKIEWICZ[32], D.F. START, C.A. STEED, D. STORK, P.E. STOTT, P. STUBBERFIELD, D. SUMMERS, H. SUMMERS[13], L. SVENSSON, J.A. TAGLE[33], M. TALBOT, A. TANGA, A. TARONI, C. TERELLA, A TERRINGTON, A TESINI, P.R. THOMAS, E. THOMPSON, K. THOMSEN, F. TIBONE, A. TISCORNIA, P. TREVALION, B. TUBBING, P. VAN BELLE, H. VAN DER BEKEN, G. VLASES, M. VON HELLERMANN, T. WADE, C. WALKER, R. WALTON[31], D. WARD, M.L. WATKINS, N. WATKINS, M.J. WATSON, S. WEBER[34], J. WESSON, T.J. WIJNANDS, J. WILKS, D. WILSON, T. WINKEL, R. WOLF, D. WONG, C. WOODWARD, Y. WU[35], M. WYKES, D. YOUNG, I.D. YOUNG, L. ZANNELLI, A. ZOLFAGHARI[19], W. ZWINGMANN

[1] Harwell Laboratory, UKAEA, Harwell, Didcot, Oxfordshire, UK.
[2] Risø National Laboratory, Roskilde, Denmark.
[3] Institute for Aerospace Studies, University of Toronto, Downsview, Ontario, Canada.
[4] ENEA Frascati Energy Research Centre, Frascati, Rome, Italy.
[5] University of Leicester, Leicester, UK.
[6] Oak Ridge National Laboratory, Oak Ridge, TN, USA.
[7] Royal Institute of Technology, Stockholm, Sweden.
[8] I.V. Kurchatov Institute of Atomic Energy, Moscow, Russian Federation.
[9] Queens University, Belfast, UK.
[10] University of Essex, Colchester, UK.
[11] Culham Laboratory, UKAEA, Abingdon, Oxfordshire, UK.
[12] Imperial College of Science, Technology and Medicine, University of London, London, UK.
[13] University of Strathclyde, Glasgow, UK.
[14] Keldysh Institute of Applied Mathematics, Moscow, Russian Federation.
[15] FOM-Institute for Plasma Physics "Rijnhuizen", Nieuwegein, Netherlands.
[16] Institute of Plasma Physics, Academia Sinica, Hefei, Anhui Province, China.
[17] National Institute for Fusion Science, Nagoya, Japan.
[18] Soltan Institute for Nuclear Studies, Otwock/Świerk, Poland.
[19] Plasma Fusion Center, Massachusetts Institute of Technology, Boston, MA, USA.
[20] Nuclear Engineering Laboratory, Lappeenranta University, Finland.
[21] A.F. Ioffe Physico-Technical Institute, St. Petersburg, Russian Federation.
[22] Max-Planck-Institut für Plasmaphysik, Garching, Germany.
[23] Department of Physics, University of Milan, Milan, Italy.
[24] Universidad Complutense de Madrid, Madrid, Spain.
[25] North Carolina State University, Raleigh, NC, USA.
[26] Dartmouth College, Hanover, NH, USA.
[27] Central Research Institute for Physics, Budapest, Hungary.
[28] University of Lund, Lund, Sweden.
[29] Laboratorio Nacional de Engenharia e Tecnologia Industrial, Sacavem, Portugal.
[30] Institute of Mathematics, University of Oxford, Oxford, UK.
[31] Princeton Plasma Physics Laboratory, Princeton University, Princeton, NJ, USA.
[32] RCC Cyfronet, Otwock/Świerk, Poland,
[33] Centro de Investigaciones Energéticas, Medioambientales y Tecnológicas, Madrid, Spain.
[34] Freie Universität, Berlin, Germany.
[35] Insitute for Mechanics, Academia Sinica, Beijing, China.